

Copper(II) Complexes of Phenanthroline and Histidine Containing Ligands: Synthesis, Characterization and Evaluation of their DNA Cleavage and Cytotoxic Activity

Sílvia M. G. Leite,[†] Luís M. P. Lima,[†] Sofia Gama,^{‡,#} Filipa Mendes,[‡] Maylis Orio,[§] Isabel Bento,^{†,||} António Paulo,[‡] Rita Delgado,[†] and Olga Iranzo^{*,†,§}

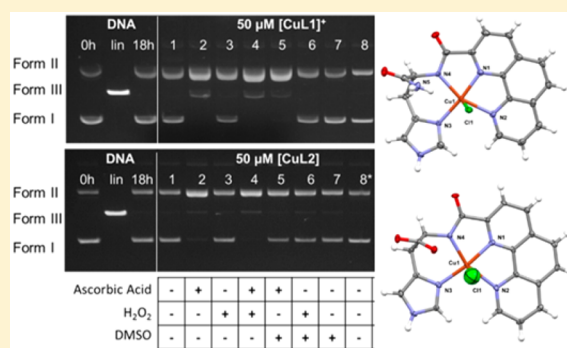
[†]Instituto de Tecnologia Química e Biológica António Xavier, Universidade Nova de Lisboa, Avenida da República, 2780-157 Oeiras, Portugal

[‡]Centro de Ciências e Tecnologias Nucleares, IST, Universidade de Lisboa, Estrada Nacional 10, 2695-066 Bobadela LRS, Portugal

[§]Aix Marseille Univ, CNRS, Centrale Marseille, iSm2, Marseille, France

Supporting Information

ABSTRACT: Copper(II) complexes have been intensely investigated in a variety of diseases and pathological conditions due to their therapeutic potential. The development of these complexes requires a good knowledge of metal coordination chemistry and ligand design to control species distribution in solution and tailor the copper(II) centers in the right environment for the desired biological activity. Herein we present the synthesis and characterization of two ligands HL1 and H₂L2 containing a phenanthroline unit (phen) attached to the amino group of histidine (His). Their copper(II) coordination properties were studied using potentiometry, spectroscopy techniques (UV–vis and EPR), mass spectrometry (ESI-MS) and DFT calculations. The data showed the formation of single copper complexes, [CuL1]⁺ and [CuL2], with high stability within a large pH range (from 3.0 to 9.0 for [CuL1]⁺ and from 4.5 to 10.0 for [CuL2]). In both complexes the Cu²⁺ ion is bound to the phen unit, the imidazole ring and the deprotonated amide group, and displays a distorted square pyramidal geometry as confirmed by single crystal X-ray crystallography. Interestingly, despite having similar structures, these copper complexes show different redox potentials, DNA cleavage properties and cytotoxic activity against different cancer cell lines (human ovarian (A2780), its cisplatin-resistant variant (A2780cisR) and human breast (MCF7) cancer cell lines). The [CuL2] complex has lower reduction potential ($E_{pc} = -0.722$ V vs -0.452 V for [CuL1]⁺) but higher biological activity. These results highlight the effect of different pendant functional groups (carboxylate vs amide), placed out of the coordination sphere, in the properties of these copper complexes.



INTRODUCTION

Copper is a biologically active metal ion that presents unique hydrolytic and redox activities. Additionally, Cu²⁺ is a d⁹ metal ion with borderline Lewis acid properties,¹ and therefore, capable of binding to different donor atoms present in biomolecules and forming complexes with diverse coordination numbers and geometries. These properties make copper an essential cofactor in many enzymes that are critical for life as well as a key component in a myriad variety of biological functions.^{2–7} However, it is its redox activity that also renders copper potentially toxic because it can promote the formation of reactive oxygen species (ROS).^{5,8,9} This double-edged sword behavior has interested researchers for long time and copper complexes and copper molecular systems have been developed and their properties harnessed for the development of unique biological, catalytic, diagnostic and therapeutic applications. In the medicinal inorganic chemistry community, the therapeutic drawbacks encountered by the complexes of platinum and

platinum group metals as anticancer drugs have awakened a quest for the development of alternatives strategies to obtain transition biometal-based drugs with improved pharmacological properties. In this regards, copper coordination compounds have become very appealing and not surprisingly, numerous copper complexes have been developed targeting a broad spectrum of diseases and recently nicely reviewed.^{10–16}

The development of these complexes requires a good knowledge of metal coordination chemistry and ligand design to control and tune the properties of copper, as well as to control the species distribution as a function of pH. Obtaining single copper complexes with the desired stability in specific pH ranges is important and allows a better knowledge of the potential active species in the different processes under study. Under these premises, we are interested in designing ligands

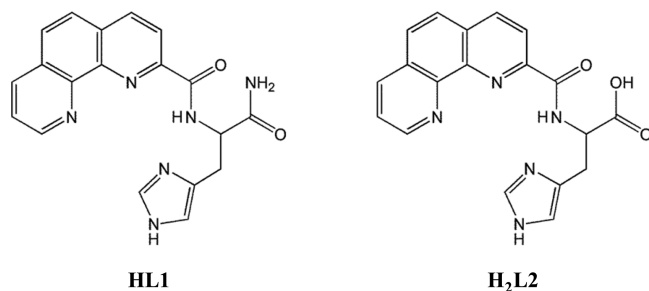
Received: August 3, 2016

Published: November 7, 2016

that contain a phenanthroline (phen) unit, a well-known copper chelator,¹⁷ in combination with amino acids, in this specific case histidine (His). This amino acid plays a crucial role in copper coordination to peptides and proteins acting as a nucleation site and generating complexes with high thermodynamic stability. This stability can be reinforced by the copper induced deprotonation of the adjacent backbone amides.^{5,18–20} Numerous phen containing copper complexes have been reported as anticancer agents¹⁵ since the initial discovery of the nuclease activity of Cu(phen)₂ by Sigman and co-workers.^{21,22} Their action relies mainly in oxygen activation and DNA oxidation. Within these complexes, some combine the phen unit with amino acids as independent units forming ternary complexes. Namely, the copper complexes known as Casiopeínas, developed by Ruiz-Azuara and co-workers,^{23–28} and Casiopeína-like compounds.^{29–42} These complexes have the general formulas [Cu(N–N)(N–O)]⁺ and [Cu(N–N)(O–O)]⁺, where N–N is an aromatic substituted diamine (phen, bipyridine and extended planar heterocyclic bases), N–O is an α -L-amino acidato and O–O is acetylacetonate or salicylaldehyde. Different amino acids have been tested, among them L-glycine, L-alanine, L-valine, L-leucine, L-isoleucine, L-proline, L-phenylalanine, L-tryptophan, L-tyrosine, L-threonine, L-methionine, L-ornithine, and L-arginine. Generally, these complexes bind and cleave DNA via ROS generation and the effect of changing the nature of the amino acid unit on biological activity is less pronounced that the effect of changing the aromatic substituted diamine.^{15,27}

Since the oxidative and hydrolytic cleavage efficiency of metallonucleases are directly affected by several factors, among them the features of the ligand and the pH, we were interested on studying ligands containing the phen unit and the amino acid His in a single molecule. We hypothesized that this design will allow a more precise control over the formation of different copper(II) species as a function of pH. Additionally, we were interested to investigate the effect of the replacement of the carboxylic group of His by an amide one on the final properties of the copper complexes. Within this context, the ligands HL and H₂L2 (Scheme 1) were prepared.

Scheme 1. Schematic Representation of the Ligands Studied in This Work



The aim of this work is therefore to characterize the copper(II) complexes of HL1 and H₂L2 using different methodologies, namely, potentiometry, X-ray crystallography, mass spectrometry, and spectroscopy, and to analyze their redox behavior, DNA cleavage properties and cytotoxic activity. Interestingly, even though both ligands are alike and their copper(II) complexes have similar properties in solution, their redox potentials and activities are different reflecting the

influence of having an amide C-terminal (HL1) versus a carboxylic C-terminal (H₂L2).

RESULTS AND DISCUSSION

Synthesis of the HL1 and H₂L2 Ligands. The ligands HL1 and H₂L2 were prepared using standard solid phase peptide synthesis protocols.⁴³ The 2-carboxy-1,10-phenanthroline unit was obtained as previously described,⁴⁴ and it was coupled to the His-bound resin using the PyBOP/DIEA activation method rather than the HBTU/HOBt/DIEA alternative, which generated lower yields. After deprotection and removal from the resin support, the crude ligands were dissolved in the minimum amount of ethanol and precipitated with hydrochloric acid to obtain the pure corresponding salts.

Protonation Constants of the HL1 and H₂L2 Ligands. The protonation constants of the two ligands were determined by potentiometric titrations in aqueous solution at 298.2 K and ionic strength 0.10 M in KNO₃. The data are presented in Table 1 and the corresponding experimental titration curves and species distribution diagrams are represented in Figures S1 and S2, respectively. Two protonation constants were determined for HL1 and a total of three were observed for the counterpart H₂L2. In both ligands, the first protonation constant can be assigned to the protonation of the imidazole (im) group and the second one to the protonation of the phen unit. In the case of H₂L2, the third constant corresponds to the protonation of the carboxylate group.

As usual the amide groups of both ligands could not be deprotonated in aqueous solution at the pH range possible to have reliable values by potentiometry. The data show that the protonation constants of the im ring and phen unit in H₂L2 are higher than those determined for HL1. This different behavior can be ascribed to the presence of the carboxylate group in the H₂L2 ligand that may stabilize the protonated im ring and phen unit. Consistent with this, the value determined for the protonation of the carboxylate group in H₂L2 is lower than the expected one for acetic acid ($\log K = 4.6$)⁴⁵ indicating that this group could be involved in H bonds O[−]⋯H–N mainly with neighboring protonated im ring, and in less extend to the phen unit ($\log K$ for the phen group is 4.93 in similar conditions)⁴⁶ or the amide group.

Stability Constants and Speciation of the Copper(II) Complexes with HL1 and H₂L2. The stability constants for the formation of the copper(II) complexes with HL1 and H₂L2 were also determined by potentiometric titrations at the experimental conditions described for the protonation constants (experimental titration curves are shown in Figure S1). The determined values for the overall ($\log \beta_{\text{CuH}_n\text{L}}$) and the calculated stepwise ($\log K_{\text{CuH}_n\text{L}}$) formation constants are collected in Table 2, and the speciation diagrams are represented in Figure 1. Only mononuclear complexes of type CuH_nL were found for both ligands.

The speciation diagrams indicate that at 1:1 Cu²⁺:ligand ratio the concentration of free Cu²⁺ ion is practically zero in solution at pH values > 3.5 and 4.0 for HL1 and H₂L2, respectively. Only one protonated species is observed for H₂L2 ([CuHL2]⁺) at low pH values up to pH 5, which indicates that the amide as well as the im groups of HL1 are immediately deprotonated upon coordination to the metal ion. The complex [CuL1]⁺ is the only species in solution up to pH about 9 while [CuL2]⁺ predominates between pH 4.5 to 10. At pH about 9.5 one water molecule coordinated directly to the copper center starts

Table 1. Overall (β_i^H) and Stepwise (K_i^H) Protonation Constants of the HL1 and H₂L2 Ligands in Aqueous Solution at $T = 298.2 \pm 0.1$ K and $I = 0.10 \pm 0.01$ M in KNO₃

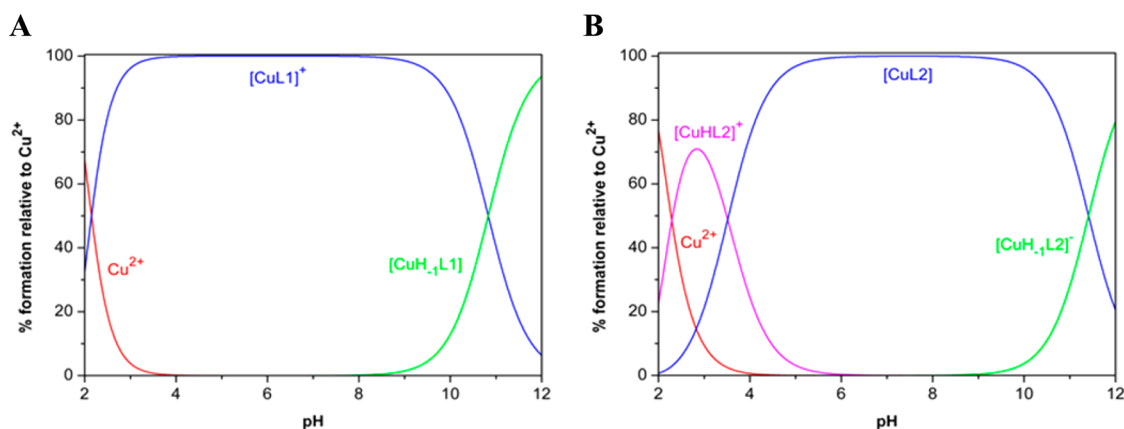
equilibrium reaction	$\log \beta_i^{H^a}$	equilibrium reaction	$\log K_i^H$
$HL1 + H^+ \rightleftharpoons H_2L1^+$	6.58(1)	$HL1 + H^+ \rightleftharpoons H_2L1^+$	6.58
$HL1 + 2 H^+ \rightleftharpoons H_3L1^{2+}$	10.56(1)	$H_2L1^+ + H^+ \rightleftharpoons H_3L1^{2+}$	3.98
$HL2^- + H^+ \rightleftharpoons H_2L2$	7.09(1)	$HL2^- + H^+ \rightleftharpoons H_2L2$	7.09
$HL2^- + 2 H^+ \rightleftharpoons H_3L2^+$	11.42(1)	$H_2L2 + H^+ \rightleftharpoons H_3L2^+$	4.33
$HL2^- + 3 H^+ \rightleftharpoons H_4L2^{2+}$	13.56(2)	$H_3L2^+ + H^+ \rightleftharpoons H_4L2^{2+}$	2.14

^aValues in parentheses are standard deviations in the last significant figures.

Table 2. Overall ($\log \beta_{CuH_nL}$) and Stepwise ($\log K_{CuH_nL}$) Stability Constants of the Copper(II) Complexes of HL1 and H₂L2 in Aqueous Solution at $T = 298.2 \pm 0.1$ K and $I = 0.10 \pm 0.01$ M in KNO₃

equilibrium reaction	$\log \beta_{CuH_nL}^a$	equilibrium reaction	$\log K_{CuH_nL}$
$Cu^{2+} + HL1 \rightleftharpoons [CuL1]^+ + H^+$	7.42(1)	$[CuL1]^+ + H^+ \rightleftharpoons [CuHL1]^{2+}$	7.42
$Cu^{2+} + HL1 \rightleftharpoons [CuH_{-1}L1] + 2 H^+$	-3.41(1)	$[CuL1]^+ \rightleftharpoons [CuH_{-1}L1] + H^+$	10.83
$Cu^{2+} + HL2^- \rightleftharpoons [CuHL2]^+$	10.43(1)	$Cu^{2+} + HL2^- \rightleftharpoons [CuHL2]^+$	10.43
$Cu^{2+} + HL2^- \rightleftharpoons [CuL2] + H^+$	6.92(1)	$[CuL2] + H^+ \rightleftharpoons [CuHL2]^+$	3.51
$Cu^{2+} + HL2^- \rightleftharpoons [CuH_{-1}L2]^- + 2 H^+$	-4.49(1)	$[CuH_{-1}L2]^- + H^+ \rightleftharpoons [CuL2]$	11.41

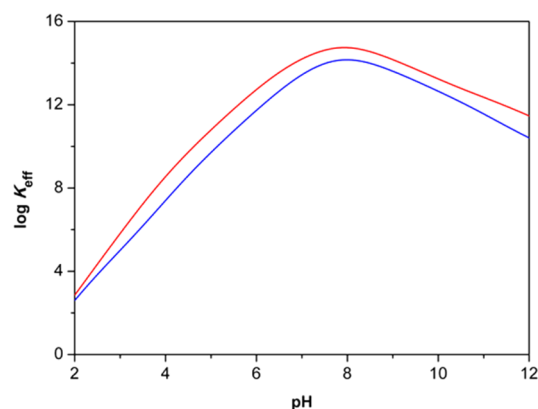
^aValues in parentheses are standard deviations in the last significant figure.

**Figure 1.** Species distribution diagrams for the copper(II) complexes of the HL1 (A) and H₂L2 (B) in aqueous solution, at 298.2 K, $I = 0.1$ M KNO₃, $C_{HL1} = C_{H_2L2} = C_{Cu} = 1.0 \times 10^{-3}$ M.

to be deprotonated for both ligands forming the CuLOH ([CuH₋₁L1] and [CuH₋₁L2]⁻), which is a usual pH value for this type of hydrolysis.⁴⁷

To compare the complexometric behavior of both ligands for copper(II), the effective constants ($K_{\text{eff}} = \frac{\text{conc. all complex species}}{(\sum \text{conc. ligand species not bound to copper}) \times (\sum \text{conc. copper species not bound to ligand})}$) were calculated using the HySS program⁴⁸ and taking into account the different protonation constants of the ligands (Figure 2). The data show that both ligands form strong complexes with Cu²⁺, with HL1 being slightly stronger than H₂L2 in the entire pH range. Both complexes have maximum K_{eff} values at about pH 7.7.

The structure of HL1 is so well tailored to the coordination of copper(II) that this metal ion is able to remove all ligand protons, even the amide one, to form the [CuL1]⁺ complex from about pH 1. Deprotonation of the amide group at low pH values have been previously reported in cases where fused chelate ring are simultaneously being formed.⁵ In the case of H₂L2, one protonated species [CuHL2]⁺ remains with $\log K = 3.51$. This value is higher than the protonation of the carboxylate and lower than the one of the phen group of the free ligand. These features indicate that the carboxylate group is out of the coordination sphere and almost undisturbed by the

**Figure 2.** Values of $\log K_{\text{eff}}$ in function of the pH for the copper(II) solutions of HL1 (red) and H₂L2 (blue) taking into account the values of Tables 1 and 2. $C_{HL1} = C_{H_2L2} = C_{Cu} = 1.0 \times 10^{-3}$ M.

charge effect of the metal center. Therefore, the metal coordination will remove all the protons of H₂L2 except the one of the carboxylate group, and as the im group is already involved in the coordination to copper center, the carboxylate

cannot be stabilized by hydrogen bonds, which justify the higher protonation constant of the $[\text{CuHL2}]^+$ complex. As discussed below, the single crystals structures and all the spectroscopic measurements confirmed these points.

The comparison of the strength of the copper(II) chelation between our ligands and some studied Casiopeínas would be very interesting. However, to the best of our knowledge we could not find any value of stability constants or K_{eff} from the recent literature. Looking to the old literature we found stability constants for two His derivatives, having a picolinyl (Pic) or a L-pyrroglutamyl (Pyr) groups replacing the phen group of our ligands,⁴⁹ and ternary complexes formed by phen and an additional ligand such as Acac (acetylacetonone), Salal (salicylaldehyde), Gly (glycine), and Tyr (tyrosine),⁵⁰ (see Figure S3 for the schematic representation of these ligands). With these values and the corresponding protonation constants of all the ligands it was possible to create the diagram represented in Figure S4. This diagram clearly shows that HL1 and H₂L2 exhibit, at the physiologic pH (7.4), the larger values of 14.55 and 13.89 (in log units), respectively, followed by phenAcac ($\log K_{\text{eff}} = 12.87$), PicHis ($\log K_{\text{eff}} = 12.48$), phenSalal ($\log K_{\text{eff}} = 11.51$), phenGly ($\log K_{\text{eff}} = 11.38$), phenTyr ($\log K_{\text{eff}} = 9.86$) and finally PyrHis ($\log K_{\text{eff}} = 6.14$). It is not surprising to verify that our ligands are the best chelators for copper(II) due to the chelate effect derived from the design of the compounds when compared with ternary complexes, or the best chelating properties of the phen group when compared with Pic or Pyr.

Characterization of the $[\text{CuL1}]^+$ and $[\text{CuL2}]$ Complexes. The $[\text{CuL1}]^+$ and $[\text{CuL2}]$ complexes were characterized using different spectroscopic techniques, mass spectrometry, and X-ray crystallography.

Vis Spectroscopy. The absorption spectra in the Vis region of $[\text{CuL1}]^+$ and $[\text{CuL2}]$ complexes recorded at pH 7.4 are shown in Figure 3. In both cases, an absorption band

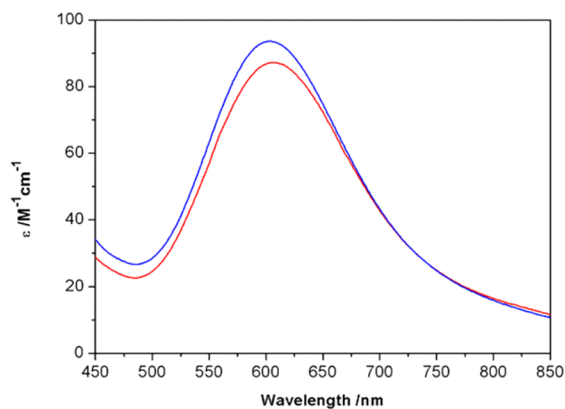


Figure 3. Vis spectra of the $[\text{CuL1}]^+$ (red line) and $[\text{CuL2}]$ (blue line) complexes at 5.0×10^{-4} M, 298.2 K, and pH 7.4.

corresponding to the Cu^{2+} d–d transitions is observed in the spectral window from 450 to 800 nm. The wavelengths and molar absorptivity coefficients of the maximum absorbance are reported in Table 3. These values are very similar which is consistent with an analogous equatorial coordination environment (phen, im and deprotonated amide).

The spectrum of $[\text{CuL1}]^+$ did not change from pH 3.0 to 11.0 indicating the presence of the same major species in that pH range. For the copper(II) complex of H₂L2, a small change was observed at pH 3.0 consistent with the presence of the protonated species $[\text{CuHL2}]^+$ (Figures 1B and S5).

Table 3. Spectroscopic Data for the $[\text{CuL1}]^+$ and $[\text{CuL2}]$ Complexes at pH 7.4

spectroscopy	$[\text{CuL1}]^+$	$[\text{CuL2}]$
vis		
λ_{max} (nm), ϵ ($\text{M}^{-1}\text{cm}^{-1}$)	606, 87	602, 94
EPR		
A_1 ($\times 10^{-4}$ cm^{-1})	175.4	175.2
A_2 ($\times 10^{-4}$ cm^{-1})	16	12
A_3 ($\times 10^{-4}$ cm^{-1})	2	2
g_1	2.219	2.218
g_2	2.07	2.07
g_3	2.04	2.04

EPR Spectroscopy. The X-band EPR spectra of the copper(II) complexes of HL1 and H₂L2 were recorded at pH 3.0, 7.4, and 11.0 (12.0 for the latter complex) in glassy water/dimethyl sulfoxide (9:1, v:v) solutions at 90 K (Figures 4 and

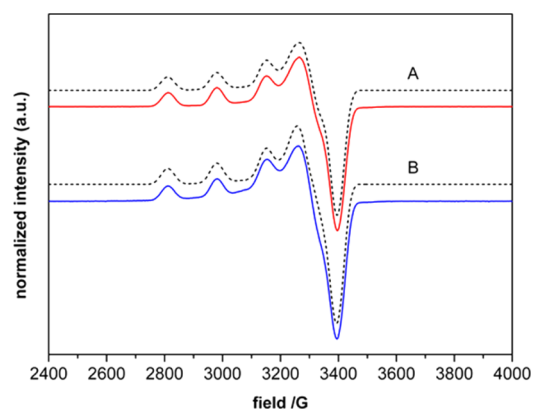


Figure 4. X-band EPR spectra of the copper(II) complexes of HL1 (A) and H₂L2 (B) in water/DMSO (9:1, v:v) at pH 7.4 and 90 K. Dashed lines represent the simulated spectra.

S6). The EPR parameters obtained by simulation are presented in Table 3 and the corresponding simulated spectra are shown in Figure 4 for the solutions at pH 7.4.⁵¹ The spectra display the lines expected at low field derived from the hyperfine interaction between the unpaired electron of the complex and the copper nucleus. Simulation of the spectra using a single paramagnetic species lead to three different principal g values with $g_1 > g_2 \sim g_3$. Such values are characteristic for rhombic mononuclear copper(II) complexes displaying elongation of the axial bonds and a $3d_{x^2-y^2}$ electronic ground state. This indicates that both complexes exist in solution on a single structural conformation. Taken into account the Vis spectra and the number of available donor atoms at this pH, square planar or square pyramidal (in case a water molecule or one anion is directly coordinated to the copper center) geometries are likely with an N4 coordination sphere that it is very similar for both complexes. The g_z and A_z values lie in the range of values reported for CuN4 systems.^{52–54} Spectra recorded at acidic and basic pH were very similar to those at pH 7.4 for both copper(II) complexes (Figure S6), displaying barely any change with pH. This feature points to analogous equatorial coordination environments in the studied pH range for the two complexes, corroborating the indications given by the vis spectra.

Electrospray Ionization Mass Spectrometry (ESI-MS). The ESI-MS spectra (positive detection mode) corresponding to

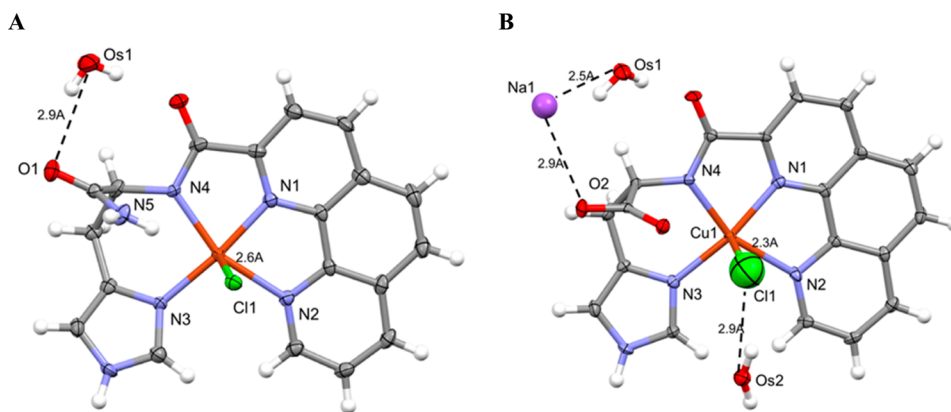


Figure 5. X-ray structures of $[\text{CuL1}(\text{Cl})\cdot\text{H}_2\text{O}]$ (A) and $[\text{Cu}(\text{NaL2}) (\text{Cl})\cdot 2\text{H}_2\text{O}]$ (B). ORTEP view⁵⁵ with thermal ellipsoids drawn at 50% probability level.

the $[\text{CuL1}]^+$ and $[\text{CuL2}]$ complexes were recorded in water/ethanol (8:2, v/v) and are shown in Figure S7. The spectrum for the $[\text{CuL1}]^+$ complex shows two single charged molecular ions at m/z 421.9 (major) and 479.8 (minor) that can be assigned to the species $[\text{HL1} + \text{Cu}^{2+} - \text{H}^+]^+$ (calcd.: 422.0 Da) and $[\text{HL1} + \text{Cu}^{2+} - \text{H}^+ + \text{Na}^+ + \text{Cl}^-]^+$ (calcd.: 480.0 Da), respectively. Na^+ (NaOH) and Cl^- (CuCl_2) ions were employed for the synthesis of the complex. The ESI-MS spectrum for the $[\text{CuL2}]$ complex shows a single charged molecular ion at m/z 422.9 corresponding to the species $[\text{H}_2\text{L2} + \text{Cu}^{2+} - \text{H}^+]^+$ (calcd.: 423.0 Da). In all cases, the peaks present the characteristic isotopic pattern of Cu^{2+} (65% ^{63}Cu and 35% ^{65}Cu) confirming the presence of the metal ion.

X-ray Crystallography. Single crystals suitable for X-ray crystallography were obtained by the slow evaporation of concentrated ethanol solutions. Crystals of both copper(II) complexes, $[\text{CuL1}(\text{Cl})]$ and $[\text{Cu}(\text{NaL2}) (\text{Cl})\cdot 2\text{H}_2\text{O}]$, belong to the orthorhombic space group ($P2_12_12_1$) with one molecule per asymmetric unit (Table 7, Experimental Section). Both complexes show a square pyramidal geometry with a distorted equatorial plane formed by the deprotonated amide, imidazole and phen nitrogen atoms of the ligands (Figure 5). A chloride ion occupies the axial position, positioned ~ 2.6 Å from the copper in the $[\text{CuL1}(\text{Cl})\cdot\text{H}_2\text{O}]$ complex (Figure 5A). In the case of $[\text{Cu}(\text{NaL2}) (\text{Cl})\cdot 2\text{H}_2\text{O}]$ complex, the chloride ion seats ~ 2.3 Å away from the copper atom, interacting also with an oxygen atom of a symmetry related water molecule (~ 2.9 Å). In addition, in this complex, a sodium ion was observed interacting with the deprotonated carboxylate group (~ 2.9 Å) and with the other water molecule (~ 2.5 Å) (Figure 5B).

Selected bond lengths and angles are shown in Table 4. The Cu–N1 (phen nitrogen) distances are 0.211 ($[\text{CuL1}(\text{Cl})\cdot\text{H}_2\text{O}]$) and 0.233 ($[\text{Cu}(\text{NaL2}) (\text{Cl})\cdot 2\text{H}_2\text{O}]$) Å shorter than those of the respective Cu–N2 (phen nitrogen) distances according to the electronegative character of the trans ligand: imidazole ring for Cu–N1 bond and amidate for Cu–N2 bond. Overall, the Cu–N1 and Cu–N2 bonds are shorter in the $[\text{CuL1}(\text{Cl})\cdot\text{H}_2\text{O}]$ complex than those in the $[\text{Cu}(\text{NaL2}) (\text{Cl})\cdot 2\text{H}_2\text{O}]$ counterpart while the reverse situation is observed for the Cu–Cl distance. Both complexes have a distorted square pyramidal geometry as observed for the Casiopeínas and other related complexes containing phen unit. Nonetheless, the Cu–N1 and Cu–N2 bonds are shorter and larger, respectively, than those observed in those complexes (1.968–2.052 Å).^{29–31,33,36,37,39,42,56–60} This is most likely the consequence

Table 4. Selected Bond Lengths and Bond Angles for $[\text{CuL1}(\text{Cl})]\cdot\text{H}_2\text{O}$ and $[\text{Cu}(\text{NaL2}) (\text{Cl})\cdot 2\text{H}_2\text{O}]$ Complexes

	$[\text{CuL1}(\text{Cl})]\cdot\text{H}_2\text{O}$	$[\text{Cu}(\text{NaL2}) (\text{Cl})\cdot 2\text{H}_2\text{O}$
bond lengths (Å)		
Cu1–N1	1.935(4)	1.943(3)
Cu1–N2	2.146(4)	2.176(3)
Cu1–N3	1.963(4)	1.999(3)
Cu1–N4	2.009(4)	1.969(4)
Cu1–Cl1	2.628(1)	2.314(3)
bond angles (deg)		
N1–Cu1–N2	79.1(2)	78.2(1)
N2–Cu1–N3	105.2(2)	106.3(1)
N3–Cu1–N4	95.6(2)	94.9(1)
N4–Cu1–N1	78.8(2)	79.6(1)
N1–Cu1–Cl1	96.1(1)	101.2(1)
N2–Cu1–Cl1	88.2(1)	89.0(1)
N3–Cu1–Cl1	93.0(1)	93.6(1)
N4–Cu1–Cl1	102.0(1)	96.6(1)

of the five-member ring that is formed upon binding of copper to the amidate group.

Cyclic Voltammetry. Cyclic voltammetry was carried out to study the electrochemical properties of the $[\text{CuL1}]^+$ and $[\text{CuL2}]$ complexes in aqueous solution at pH 7.4 and in 0.1 M KNO_3 as supporting electrolyte. The cyclic voltammograms of solutions containing only the ligands in the supporting electrolyte did not show any signals indicating that the ligands are not electroactive in the studied potential range (-1.0 to 0.8 V). On the other hand, the copper(II) complexes are electroactive. The cyclic voltammogram of $[\text{CuL1}]^+$ complex (Figure 6, red line) shows a cathodic ($E_{\text{pc}} = -0.452$ V) and an anodic peak ($E_{\text{pa}} = 0.201$ V) with a peak to peak separation $\Delta E_{\text{p}} = E_{\text{pa}} - E_{\text{pc}} = 0.653$ V. The cyclic voltammetric behavior of the $[\text{CuL2}]$ complex is similar (Figure 6, blue line) showing also a cathodic ($E_{\text{pc}} = -0.722$ V) and an anodic peak ($E_{\text{pa}} = 0.181$ V) with a $\Delta E_{\text{p}} = 0.903$ V. For this complex, the reduction occurs at a more negative potential. Successive scans were performed in both systems and no changes were observed either in the cathodic or anodic peaks. These data suggest that no disproportionation reaction occurs as a consequence of the reduction of Cu^{2+} to Cu^+ . The peak currents ratio, $I_{\text{pc}}/I_{\text{pa}}$, is equal to 1 and the I_{pc} and I_{pa} show a linear variation with the square root of the scan rate (Figure S8 and Table S1) indicating that the process is diffusion controlled.⁶¹

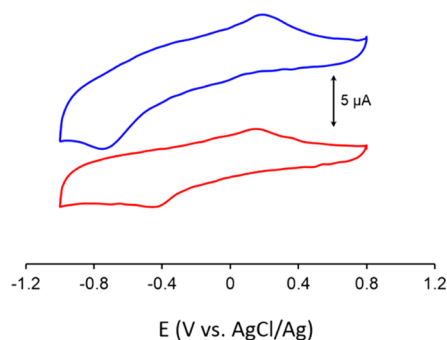


Figure 6. Cyclic voltammograms of the $[\text{CuL1}]^+$ (red) and $[\text{CuL2}]$ (blue) complexes (5.0×10^{-4} M) at pH 7.4 in solutions containing 0.10 M KNO_3 as supporting electrolyte. Scan rate: 100 mV/s.

These data reveals that the two copper(II) complexes $[\text{CuL1}]^+$ and $[\text{CuL2}]$ are reducible and the redox reaction can be ascribed to the process $\text{Cu}^{2+} \rightleftharpoons \text{Cu}^+$. In both cases, the large separation observed between the cathodic and the anodic peaks indicates a behavior characteristic of a nonreversible one electron redox process since the differences between the peaks are much higher than the expected 0.060 V for a fully reversible one-electron process. This shows that a chemical reaction is coupled with the electron transfer leading to the nonreversibility. These changes correspond most likely to reversible changes in the coordination sphere around the copper center since no decomposition of the complexes or alteration in the cathodic and anodic peaks were observed upon several cycles. The large peak to peak separation observed will therefore reflect the structural reorganization energy necessary to accommodate the geometrical preferences of Cu^+ ion, likely tetrahedral or trigonal planar geometries. The reduction of copper(II) complexes is allowed when the copper(II) species can easily progress toward these geometries upon reduction.⁶² The most easily reducible is the $[\text{CuL1}]^+$ complex which seems to adjust better to the different geometric preferences of Cu^{2+} (square planar or square pyramidal) and Cu^+ ions than the $[\text{CuL2}]$ complex with a larger peak to peak separation. Anyhow, the rearrangements can be considered reversible in both cases because no significant changes in the cyclic voltammograms were observed after successive scans. An additional factor that cannot be rule out is the total charge of the complexes. While reduction of $[\text{CuL1}]^+$ generates a neutral complex, that of $[\text{CuL2}]$ produces a negatively charge complex.

DFT Calculations. DFT calculations were carried out to gain insights into the different redox behavior of the $[\text{CuL1}]^+$ and $[\text{CuL2}]$ complexes and investigate possible structures for the reduced complexes. The initial geometries were taken from the crystal structures reported above. The reduction potentials calculated for the $[\text{CuL1}]^+$ and $[\text{CuL2}]$ complexes are collected in Tables 5 and S2, and their DFT optimized structures, both in neutral (Cu^{2+}) and reduced (Cu^+) forms, are shown in Figures 7 ($[\text{CuL1}]^+$) and 8 ($[\text{CuL2}]$).

Because of the electrochemical nonreversibility of the one electron redox process under investigation the calculated potentials correspond to the experimental reduction potentials

and the data corroborate the lower reduction potential of the complex $[\text{CuL2}]$ ($E_{\text{pc}} = -0.772$ V vs -0.462 V for $[\text{CuL1}]^+$). The DFT optimized structures (Figures 7 and 8, Table 6) reveal a distorted square planar coordination geometry for both complexes in their Cu^{2+} redox state form. Upon reduction, the bond $\text{Cu}-\text{N2}$ becomes longer and the final Cu(I) complexes adopt structures that are closer to a distorted T-shape geometry than a distorted square planar geometry (Figures 7 and 8, Table 6). Interestingly, the bond lengths of the reduced $[\text{CuL2}]^-$ complex are overall longer than those of the reduced $[\text{CuL1}]$. These data show that the ligands HL1 and $\text{H}_2\text{L2}$ are rigid enough to avoid the formation of Cu(I) species with the preferred tetrahedral or trigonal planar geometries and this fact could be responsible for the nonreversibility of the redox process observed for the $[\text{CuL1}]^+$ and $[\text{CuL2}]$ complexes during the electrochemistry experiments. Indeed, the Casiopeínas and Casiopeína-like compounds have a more reversible behavior than the one observed in our systems. This is in agreement with the higher flexibility of these ternary complexes where the phen and amino acid units are an independent set of ligands.^{23–28,34–36}

Biological Assays. The cytotoxic and DNA cleavage activity of the $[\text{CuL1}]^+$ and $[\text{CuL2}]$ complexes were evaluated to have a first insight on their potential antitumor properties.

DNA Cleavage Evaluation. To assess the DNA cleavage activity of the ligands and corresponding Cu(II) complexes, a model DNA plasmid, supercoiled ϕX174 phage DNA, was incubated with the different compounds, in phosphate buffer (pH 7.2) for 18 h at 37 °C. The evaluation of the DNA cleavage activity was performed by monitoring the presence of different DNA isoforms via a gel electrophoresis assay: supercoiled DNA (Sc, form I), nicked circular DNA (Nck, form II), and linear DNA (Lin, form III).

Figure 9 shows the gel electrophoresis of the different DNA/compound mixtures. The Cu(II) complexes were able to induce conformational changes in plasmid DNA in a concentration-dependent manner, as the increase in concentration (up to 250 μM) of the compounds promoted an increased DNA nicking. This effect is due to the action of the complexes since no free Cu^{2+} ion is present in solution at the range of concentrations used (see Figures S9 and S10).

The interaction of the complexes with DNA gives rise to a higher proportion of nicked circular form (Form II), but no supercoiled form is detected (Form I), which points out for the occurrence of single-strand breaks without significant formation of double-strand breaks. The supercoiled/nicked circular (Sc/Nck) ratio found for control DNA (without addition of any compound) is similar to those obtained for ligands HL1 and $\text{H}_2\text{L2}$, except for $\text{H}_2\text{L2}$ at concentrations of 250 μM , where a small effect can be quantified by a decrease of the Sc/Nck ratio to about one-half of the control.

For $[\text{CuL1}]^+$ and $[\text{CuL2}]$, the activity registered is higher when compared with the corresponding ligands, with the Sc/Nck ratio decreasing to values four times smaller than the control at the highest concentration tested. However, while in case of $[\text{CuL1}]^+$ this effect is visible at concentrations equal or

Table 5. Calculated Redox Potentials for $[\text{CuL1}]^+$ and $[\text{CuL2}]$

complex	ΔG_{g}^0 (Eh)	ΔG_{sox}^0 (Eh)	ΔG_{red}^0 (Eh)	ΔG_{g}^0 (Eh)	ΔG_{g}^0 (eV)	E_{pc} (eV)
$[\text{CuL1}]^{+/0}$	-0.1927	-0.0548	-0.1090	-0.1385	-3.768	-0.462
$[\text{CuL2}]^{0/-1}$	-0.0702	-0.1425	-0.0856	-0.127	-3.458	-0.772

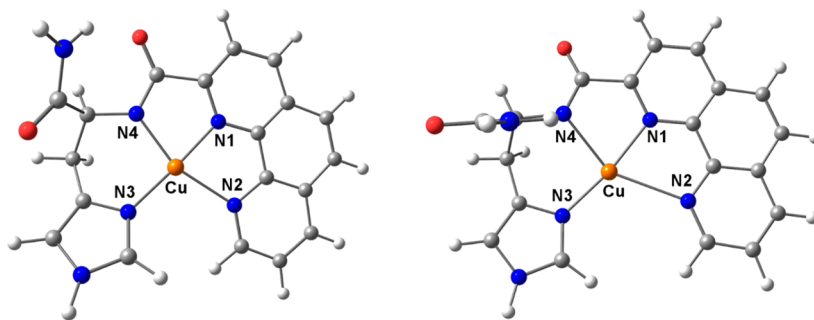


Figure 7. DFT optimized structure of $[\text{CuL1}]^+$ in its neutral (left) and reduced (right) forms. Color scheme: Cu, light brown; O, red; N, dark blue; C, gray; H, white.

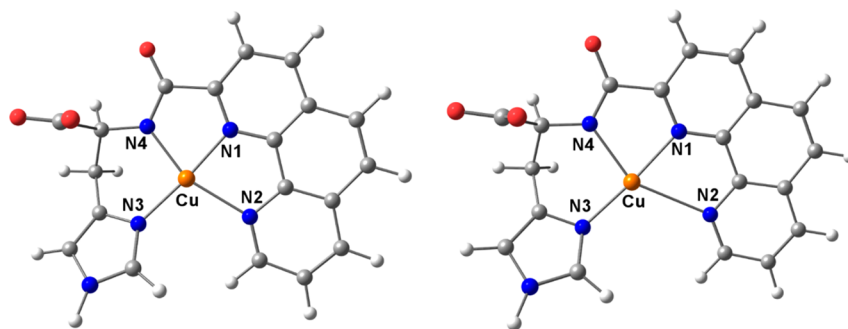


Figure 8. DFT optimized structure of $[\text{CuL2}]$ in its neutral (left) and reduced (right) forms. Color scheme: Cu, light brown; O, red; N, dark blue; C, gray; H, white.

Table 6. Selected Bond Lengths and Bond Angles for the Optimized DFT Structures of $[\text{CuL1}]^+$ and $[\text{CuL2}]$

bond lengths (Å)	Cu–N1	Cu–N2	Cu–N3	Cu–N4		
$[\text{CuL1}]^+$	1.959	2.203	1.978	2.026		
$[\text{CuL1}]$	2.042	2.538	1.975	2.217		
$[\text{CuL2}]$	1.949	2.197	1.961	2.004		
$[\text{CuL2}]^{-1}$	2.070	2.620	1.984	2.141		
bond angles (deg)	N1–Cu–N2	N2–Cu–N3	N3–Cu–N4	N4–Cu–N1	N1–Cu–N3	N2–Cu–N4
$[\text{CuL1}]^+$	78.4	106.5	95.0	79.4	172.7	156.8
$[\text{CuL1}]$	72.3	116.7	95.8	77.7	166.9	146.2
$[\text{CuL2}]$	78.6	105.8	96.0	80.0	173.6	157.9
$[\text{CuL2}]^{-1}$	70.5	114.4	96.9	78.7	173.0	148.4

higher than $100 \mu\text{M}$, in the case of $[\text{CuL2}]$ there is registered activity even at lower concentration values ($50 \mu\text{M}$).

Mechanistic Study of DNA cleavage. To obtain some insight about the cleavage pathway of the presented copper(II) complexes, further experiments were made to evaluate the effect of some activating agents such as ascorbic acid (AscH_2) and/or H_2O_2 (Figure 10).

The presence of a redox agent as ascorbic acid in the reaction system dramatically increases DNA cleavage efficiency of both copper(II) complexes (see lines 2, 4, 10, and 12 from Figure 10). The ascorbate ion (AscH^-) is the predominant species at pH 7.2 (phosphate buffer). AscH^- is able to react with molecular oxygen leading to the formation of the dehydroascorbic acid (Asc) form. This reaction is metal-catalyzed by ions such as Cu^{2+} (and Fe^{3+}) where ascorbate works as a pro-oxidant by reducing them (Scheme 2, reaction 1). The Cu^+ ion formed by the oxidation of ascorbate can then catalyze the generation of the hydroxyl radical (OH^\bullet) from H_2O_2 in Fenton like reactions (Scheme 2, reaction 2).^{63–65}

The addition of H_2O_2 to the system also shows some increase on the DNA cleavage efficiency of the studied copper(II) complexes (lines 3, 4, 11, and 12 from Figure 10). This can be a result of the reduction of $[\text{CuL1}]^+$ and $[\text{CuL2}]$ complexes to Cu^+ (reaction 3 from Scheme 2) followed by the oxidation to Cu^{2+} , again with formation of ROS species. In both instances (addition of ascorbic acid or H_2O_2), the redox cycling of $\text{Cu}^{2+}/\text{Cu}^+$ results in the formation of reactive oxygen species (ROS) that are responsible for the nuclease activity exhibited by the complexes, as indicated in Scheme 2 (reaction 5).

To clarify the presence of ROS in the cleavage mechanism, the effect of the addition of a radical scavenger was assessed. DMSO, a hydroxyl radical scavenger, was added (lines 5, 6, 13, and 14) and we could observe a significant inhibition of the cleavage process, more severe in the case of activation by ascorbic acid. This identifies the hydroxyl radical as one of the species that is involved in the strand scission property of $[\text{CuL1}]^+$ and $[\text{CuL2}]$ complexes. According with Scheme 2, the presence of hydroxyl radicals is consistent with the auto-oxidation of ascorbic acid, catalyzed by the presence of Cu^{2+} . In parallel, experiments using ascorbic acid, H_2O_2 and DMSO were also performed as a control. In the presence of ascorbic acid the nicked circular form is more abundant, due to occurrence of single-strand breaks. However, this effect is much more reduced than the one observed with the simultaneous presence of the copper(II) complexes. The presence of H_2O_2 and DMSO did not cause any apparent cleavage of DNA in the control experiments. The same experiments with these complexes were also performed in the absence of light, in order to assess the relevance of a photochemical cleavage pathway. In these cases, no effect is observed when compared with the complex without additives (lines 8 and 16).

Cytotoxicity Assays. The antiproliferative properties of the two copper(II) complexes, the corresponding ligands and

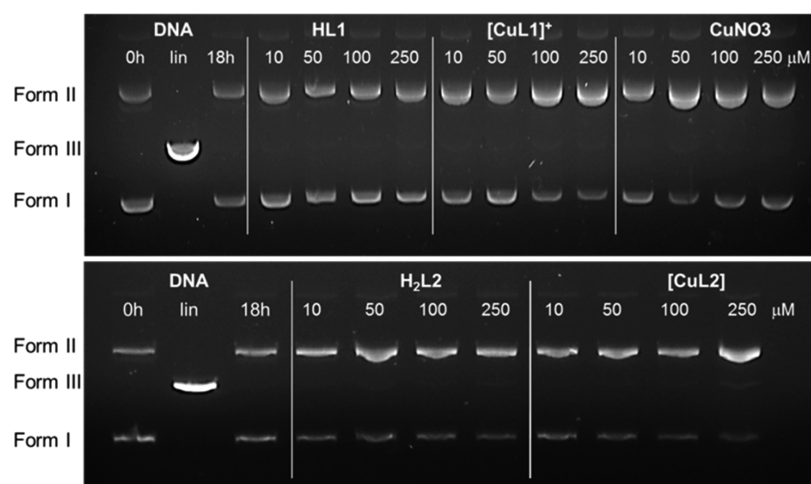


Figure 9. Cleavage of supercoiled ϕ X174 DNA by the copper(II) complexes ($[\text{CuL1}]^+$, $[\text{CuL2}]$), their ligands (HL1, H₂L2), and $\text{Cu}(\text{NO}_3)_2$ (CuNO_3), after 18 h of incubation at 37 °C in phosphate buffer (pH 7.2). DNA Lin: Linear DNA obtained by digestion with XhoI. Forms I–III are supercoiled, nicked circular, and linear forms of DNA, respectively.

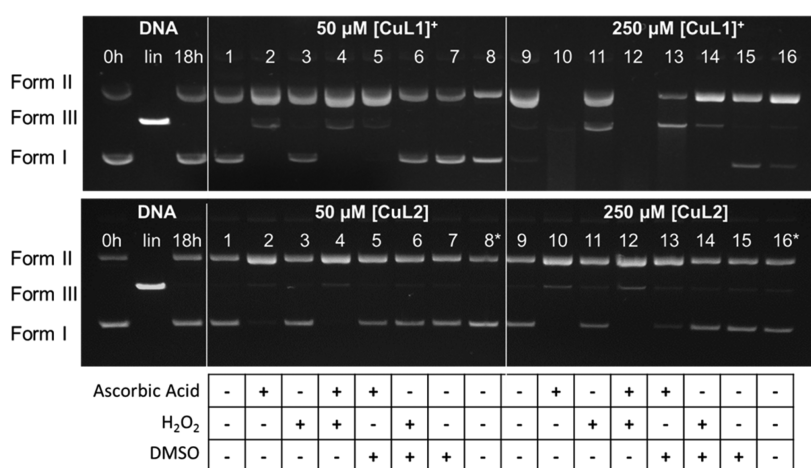
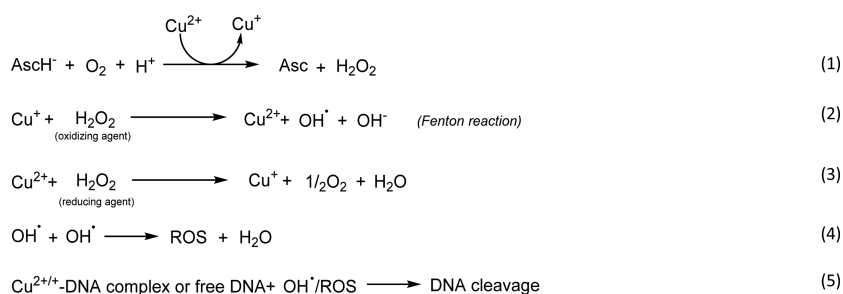


Figure 10. Cleavage of supercoiled ϕ X174 DNA by copper(II) complexes ($[\text{CuL1}]^+$ and $[\text{CuL2}]$) after 18 h of incubation at 37 °C in phosphate buffer (pH 7.2), in the presence of activating agents (ascorbic acid and H₂O₂), hydroxyl radical scavenger (DMSO) or in the dark (*). DNA lin: Linear DNA obtained by digestion with XhoI. Forms I–III are supercoiled, nicked circular, and linear forms of DNA, respectively.

Scheme 2. Proposed Pathway for the Generation of Hydroxyl Radicals and ROS Species and DNA Cleavage Mechanism



$\text{Cu}(\text{NO}_3)_2$ were assayed by monitoring their ability to inhibit cell growth. Cytotoxic activity was determined on the human ovarian cancer (A2780) cell line, its cisplatin-resistant variant (A2780cisR) and on the human breast cancer cell line (MCF7), determined by a colorimetric method (MTT assay). The activity of these new metal compounds was also compared with the activity of cisplatin in the same cell models.

Using an appropriate range of concentrations (0.002 to 200 μM), dose–response curves after long-term (72 h) exposure

were obtained. From the experimental data, the IC₅₀ values were calculated and are presented in Table 7. The HL1 and H₂L2 ligands have no cytotoxicity, however for $\text{Cu}(\text{NO}_3)_2$ there is some cytotoxic effect similarly to what we have observed previously with CuCl_2 .⁶⁶ Overall, the $[\text{CuL1}]^+$ and $[\text{CuL2}]$ complexes present low to moderate cytotoxicity in the tested cell lines, being more active against A2780 cells. In all the cell lines, the $[\text{CuL2}]$ complex shows higher cytotoxic activity than the $[\text{CuL1}]^+$. This is in agreement with its better DNA

Table 7. IC₅₀ Values for 72 h Treatment of Three Different Human Tumour Cell Lines

compound	IC ₅₀ (μM)		
	A2780	A2780cisR	MCF7
HL1	>200	>200	>200
H ₂ L2	>200	>200	>200
[CuL1] ⁺	24.24 ± 1.85	>200	>200
[CuL2]	18.01 ± 1.59	152 ± 1.86	88 ± 1.55
Cu(NO ₃) ₂	42.31 ± 1.41	91.47 ± 1.77	>200
Cisplatin	0.5 ± 0.1	16.05 ± 1.12	38 ± 1.23

cleavage properties (see previous section). However, these complexes do not overcome cisplatin cross-resistance as they are significantly less cytotoxic in the A2780cisR line. A direct and reliable comparison of the cytotoxic activity of the new complexes with the congeners of the “Casiopéinas” type is hampered by the fact that the different compounds have been tested against different cell lines with different responses to antitumor drugs. Nevertheless, the relative cytotoxicities of [CuL1]⁺ and [CuL2] are in line with the QSAR studies reported for Casiopéinas and related Cu(II) complexes that pointed out for an increasing of the biological activity for the weaker oxidants.²⁷

CONCLUSION

Copper compounds have become an interesting alternative to complexes of platinum and platinum group metals as anticancer drugs. Their development has been prompted by the aims of overcoming the therapeutic drawbacks encountered for the family of platinum drugs and of developing biometal-based drugs with improved pharmacological properties. Copper(II) complexes are much less structurally predictable than other first-row transition metal complexes due to their labile character and preference for distorted coordination geometries. Therefore, the ligand design is crucial to control and tune the properties of copper, particularly the formation of different species as a function of pH. Under these premises, two new ligands containing the amino acid His covalently attached to a phen unit, HL1 and H₂L2, were prepared, characterized and their copper(II) coordination properties analyzed in aqueous solutions.

Potentiometric studies indicate that both ligands bind copper(II) with high affinity and form single major species, [CuL1]⁺ and [CuL2], on a large pH range (from 3.0 to 9.0 and from 5.0 to 10.0, respectively). Spectroscopic data show that the Cu²⁺ ion is bound in a very similar fashion in both complexes, namely, to the deprotonated amide, the imidazole and the phen nitrogen atoms of both ligands. Single-crystal X-ray diffraction determination of these copper(II) complexes confirms these binding modes and shows the Cu center in a distorted square pyramidal geometry with a chloride ion occupying the axial position. Cyclic voltammetry shows that the [CuL1]⁺ and [CuL2] complexes are reducible and undergo a nonreversible one electron redox process, which can be ascribed to the reaction Cu²⁺ ⇌ Cu⁺. DFT calculations corroborate the lower reduction potentials determined experimentally and the DFT optimized structures reveal that the copper(I) complexes present a geometry that is closer to a distorted T-shape than a distorted square planar geometry. Overall, these data indicate that the ligands HL1 and H₂L2 are rigid enough to avoid the formation of copper(I) species with the preferred tetrahedral or trigonal planar geometries and this

factor could be responsible for the nonreversibility of the redox process. The covalent attachment of the His to the phen unit had a double impact. On one hand, it generated ligands (HL1 and H₂L2) with higher affinity for Cu²⁺ ion at pH 7.4 (log K_{eff} = 14.55 and 13.89, respectively) than that observed for related ternary complexes. On the other hand, however, it lowered the reduction potential of the [CuL1]⁺ and [CuL2] complexes producing nonreversible redox process.

Biological studies show that both copper(II) complexes are poorly active as DNA nucleases, indicating that there is a reduced contribution of hydrolytic pathways in the DNA cleavage. However, the addition of activators such as H₂O₂ or ascorbic acid enhanced the activity of the complexes, indicating the involvement of ROS in the process. The involvement of such species was confirmed by the inhibitory effect of DMSO in the cleavage. Overall, the [CuL2] complex is a more active DNA nuclease than [CuL1]⁺, which leads to higher DNA cleavage at the same metal concentration and in the absence of activators. Consistently, [CuL2] also showed higher cytotoxic activity. Taken together, the biological data reveal that the weaker oxidant, namely [CuL2], is the more active complex. This behavior was previously observed for similar ternary complexes and indicates that the covalent attachment of the His to the phen unit does not modify this trend.

We are currently modifying the HL1 and H₂L2 ligands to obtain binary copper(II) complexes with improved biological activity.

EXPERIMENTAL SECTION

Chemicals. The *N*-fluorenylmethoxycarbonyl (Fmoc)-protected amino acid Fmoc-His(Trt)-OH, rink amide MBHA resin, 2-chlorotriethyl chloride resin, 2-(1*H*-benzotriazole-1-yl)-1,1,3,3-tetraethyluronium hexafluorophosphate (HBTU) and benzotriazole-1-yl-oxy-tris-pyrrolidino-phosphonium hexafluorophosphate (PyBOP) were obtained from Novabiochem; *N*-hydroxybenzotriazole (HOBt), *N,N*-diisopropylethylamine (DIEA), trispropylsilane (TIS), acetic anhydride, piperidine, copper nitrate trihydrate (Cu(NO₃)₂·3H₂O) and copper chloride (CuCl₂) were from Sigma-Aldrich; trifluoroacetic acid (TFA) was purchased from Roth. All the other chemicals and solvents (*N,N*-dimethylformamide (DMF), diethyl ether, dichloromethane (DCM), acetonitrile (ACN), *N*-Methyl-2-pyrrolidone (NMP), chloroform (CDCl₃), and methanol (MeOH) and ethanol (EtOH) were from different commercial sources (highest available grade) and used without further purification.

Ligands and Copper Complexes Synthesis. 2-Carboxy-1,10-phenanthroline was synthesized from 1,10-Phenanthroline according to the protocol published in the literature.⁴⁴ The ligands HL1 and H₂L2 were synthesized using standard Fmoc solid-phase methods.⁴³ The electrospray ionization-mass spectra (ESI-MS) were acquired in positive mode on an ion trap mass analyzer, model LTQ (Thermo-Finnigan) by direct infusion at a flow rate of 5 μL/min. All the ESI-MS assays were performed at the Mass Spectrometry Laboratory, Analytical Services Unit of the Instituto de Tecnologia Química e Biológica, Universidade Nova de Lisboa.

HL1. This ligand was manually prepared on a rink amide MBHA resin (0.59 mmol/g, 2 g resin scale synthesis). Fmoc-His(Trt)-OH was coupled using HBTU/HOBt (3.9/4 equiv) as coupling agent, DIEA as base (8 equiv) and DMF as solvent. The 2-carboxy-1,10-phenanthroline unit was coupled using PyBOP (4 equiv) as coupling agent, DIEA as base (8 equiv) and DMF as solvent. The deprotection of the temporal Fmoc protecting group was performed by treating the resin with 20% piperidine in DMF solution. Removal of Fmoc and attachment of Fmoc-His-COOH and 2-carboxy-1,10-phenanthroline were always verified by the Kaiser-test.⁶⁷ The ligand was simultaneously deprotected and cleaved from the resin by treatment with the mixture TFA/TIS/Water (95:2.5:2.5, v/v/v, 20 mL/g of

resin) for 2 h at room temperature and under nitrogen. The resin was filtered out and rinsed with 10 mL of TFA. The filtrate and rinses were combined and concentrated under a nitrogen stream to a crude oil, from which a precipitate was obtained by addition of cold diethyl ether (20 mL). After filtration and washing with cold diethyl ether, the precipitate was redissolved in the minimum amount of ethanol and concentrated hydrochloric acid was added dropwise until a precipitate appeared. The white-beige solid was dried under vacuum. Average yield: 70%. ^1H NMR (400 MHz, D_2O) δ : 9.10 (dd, $J = 5.4$, 1.5 Hz, 1H), 9.03 (dd, $J = 8.3$, 1.5 Hz, 1H), 8.59–8.44 (m, 2H), 8.26–8.16 (m, 2H), 7.98 (s, 2H), 7.30 (d, $J = 1.4$ Hz, 1H), 4.99 (dd, $J = 8.4$, 6.4 Hz, 1H), 3.54–3.32 (m, 2H); ^{13}C NMR (100 MHz, D_2O) δ : 174.01, 164.28, 147.88, 146.44, 143.36, 138.82, 136.36, 135.54, 133.61, 130.52, 129.50, 128.96, 128.46, 126.79, 125.35, 123.15, 117.34, 52.87, 26.81; ESI-MS data: m/z 361.25 $[\text{L1} + \text{H}]^+$ (calc. for $[\text{L1} + \text{H}]^+ = 361.14$ Da), 383.17 $[\text{L1} + \text{Na}]^+$ (calc. for $[\text{L1} + \text{Na}]^+ = 383.12$ Da), 721.00 $[\text{2L1} + \text{H}]^+$ (calc. for $[\text{2L1} + \text{H}]^+ = 721.27$ Da), 743.00 $[\text{2L1} + \text{Na}]^+$ (calc. for $[\text{2L1} + \text{Na}]^+ = 743.26$ Da).

$\text{H}_2\text{L2}$. This ligand was manually assembled on a 2-chlorotriptyl chloride resin (1.22 mmol/g, 2 g resin scale synthesis) using the same protocols described above with the following changes. The Fmoc-His(Trt)-OH residue was coupled using only DIEA (2.5 equiv) in DCM solution and afterward the resin was blocked using the mixture DCM/MeOH/DIEA (80:15:5, v/v/v) during 10 min with stirring. The blocking step was repeated three times and subsequently the resin was thoroughly washed with DCM. A final white-beige solid was also obtained. Average yield: 70%. ^1H NMR (400 MHz, D_2O) δ : 9.22–9.13 (m, 2H), 8.62–8.55 (m, 1H), 8.50 (s, 1H), 8.33–8.20 (m, 2H), 8.17 (s, 2H), 7.23 (s, 1H), 4.96 (dd, $J = 8.9$, 5.2 Hz, 1H), 3.52 (dd, $J = 15.5$, 5.2 Hz, 1H), 3.34 (dd, $J = 15.5$, 8.9 Hz, 1H); ^{13}C NMR (100 MHz, D_2O) δ : 173.91, 164.66, 148.13, 146.79, 143.04, 139.01, 136.76, 136.04, 133.36, 130.94, 129.92, 129.24, 129.00, 126.86, 125.18, 123.17, 117.03, 52.61, 26.60; ESI-MS data: m/z 362.08 $[\text{L2} + \text{H}]^+$ (calc. for $[\text{L2} + \text{H}]^+ = 362.13$ Da), 384.09 $[\text{L2} + \text{Na}]^+$ (calc. for $[\text{L2} + \text{Na}]^+ = 384.11$ Da), 722.87 $[\text{2L2} + \text{H}]^+$ (calc. for $[\text{2L2} + \text{H}]^+ = 723.24$ Da), 744.94 $[\text{2L2} + \text{Na}]^+$ (calc. for $[\text{2L2} + \text{Na}]^+ = 745.22$ Da).

Copper Complexes. The same protocol was employed for the synthesis of the copper(II) complexes of HL1 and $\text{H}_2\text{L2}$. The ligand (0.5 mmol) and the CuCl_2 (0.5 mmol) were dissolved in 15 mL of ethanol and NaOH was added to adjust the apparent pH value to 6.0. The light green solution turned dark blue at this point. The solution was stirred at 60 °C during 1 h and filtered after cooling down to room temperature. The filtrate was kept at room temperature and the slow evaporation of the solvent generated the appearance of blue crystals suitable for X-ray crystallography. Only few crystals were obtained in each case and they were completely used for the X-ray determinations.

Stock Solutions. Fresh solutions of the purified ligands were prepared for each experiment using Milli-Q-water and the ligand concentration was determined by UV–vis spectroscopy using the extinction coefficient of phenanthroline determined at pH 7.4 in 100 mM Tris buffer ($\epsilon_{268\text{nm}} = 22095 \text{ M}^{-1} \text{ cm}^{-1}$) and confirmed by potentiometry. The stock solutions of $\text{Cu}(\text{NO}_3)_2$ and CuCl_2 were prepared from analytical grade metal salt and standardized by titration with $\text{K}_2\text{H}_2\text{edta}$ following standard methods.⁶⁸

Potentiometric Studies. Purified water was obtained from a Millipore Milli-Q demineralization system. Stock solutions of HL1 and $\text{H}_2\text{L2}$ ligands were prepared at $\sim 2.0 \times 10^{-3}$ M. Copper(II) nitrate solutions were prepared in water at 0.0506 M. Carbonate-free solutions of the titrant KOH were obtained at 0.0998 M by freshly prepared solution from a Merck ampule in 1000 mL of water (freshly boiled for about 2 h and allowed to cool under nitrogen). These solutions were standardized by application of Gran's method⁶⁹ and were discarded as soon as the concentration of carbonate reached ca. 1% of the total amount of base. A 0.100 M standard solution of HNO_3 prepared from a commercial ampule was used for back-titrations. The potentiometric setup used for conventional titrations was previously described.⁷⁰ The ionic strength of the experimental solutions was kept at 0.10 M with KNO_3 , temperature was controlled at 298.2 ± 0.1 K using a Grant W6/CZ1 thermostatic system and atmospheric CO_2 was excluded from the titration cell during experiments by passing purified

nitrogen across the top of the experimental solution. The $[\text{H}^+]$ of the solutions was determined by measurement of the electromotive force of the cell using the following equation:

$$E = E^\circ + Q \log[\text{H}^+] + E_j$$

The term pH is defined as $-\log[\text{H}^+]$. E° and Q were determined by titrating a solution of known hydrogen-ion concentration at the same ionic strength in the acid pH region. The liquid-junction potential, E_j , was found to be negligible under the experimental conditions used. The value of $K_w = [\text{H}^+][\text{OH}^-]$ was found to be equal to $10^{-13.78}$ by titrating a solution of known hydrogen-ion concentration at the same ionic strength in the alkaline pH region, considering E° and Q valid for the entire pH range. Measurements during titrations were carried out with 0.05 mmol of HL1 or $\text{H}_2\text{L2}$ in a total volume of 30 mL, in the absence and in the presence of 0.5 and 1 equiv of Cu^{2+} relative to the ligand concentration. A backtitration was always performed at the end of each direct complexation titration in order to check if equilibrium was attained throughout the full pH range. Each titration curve consisted typically of 90–120 points in the range of $2.5 < \text{pH} < 11.5$ and a minimum of two replicate titrations were performed for each system.

Calculation of Equilibrium Constants. The calculation of overall equilibrium constants β_i^{H} and $\beta_{\text{CuH}_i\text{L}}$ (being $\beta_{\text{CuH}_i\text{L}} = [\text{CuH}_i\text{L}]/[\text{Cu}][\text{H}]^i[\text{L}]$) was done by fitting the potentiometric data from protonation or complexation titrations with the HYPERQUAD program.⁷¹ Species distribution diagrams were plotted from the calculated constants with the HYSS program.⁴⁸ Differences, in log units, between the values of protonated or hydrolyzed and nonprotonated constants provide the stepwise reaction constants. The errors quoted are the standard deviations of the overall stability constants calculated by the fitting program from the experimental data and conditions used.

Spectroscopic Studies. Visible Spectroscopy. All the visible spectra were recorded at 298.2 K on a Varian Cary 100 Bio UV–vis Spectrophotometer equipped with a thermostated multiple cell holder and a Peltier water bath using 1 cm path length quartz cell. Samples were prepared in Milli-Q water by mixing the required amount of the stock solutions of ligand and $\text{Cu}(\text{NO}_3)_2$ to obtain 5.0×10^{-5} M final complex concentration. The final pH was adjusted to the desired value by addition of KOH or HNO_3 .

Electron Paramagnetic Resonance (EPR) Spectroscopy. The X-band EPR spectra of frozen aqueous solutions were recorded on a Bruker EMX 300 spectrometer at 90 K with the following experimental parameters: microwave power of 2.012 mW, frequency of 9.50 GHz, modulation frequency of 100 kHz, modulation amplitude of 10 G and receiver gain of 5.64×10^3 . Solutions contained 5.0×10^{-4} M of ligand and 1 equiv of $\text{Cu}(\text{NO}_3)_2$ at 3.0, 7.4, and 11.0 pH values. The experimental EPR spectra were simulated using the SpinCount software.⁵¹

ESI-Mass Spectrometry Studies of Copper Complexes. Mass spectrometric spectra of solutions (water/ethanol (8:2, v/v)) containing 0.5×10^{-3} M copper complex were acquired on Bruker Esquire 3000 plus mass spectrometer equipped with an ESI source. The instrument was operated in the positive polarity mode with a source temperature of 250 °C and a flow rate of 5 $\mu\text{L}/\text{min}$. Nitrogen was used as a drying gas at a flow rate of 5 L min^{-1} and at a constant pressure of 15 Psi. Mass spectra were acquired in an m/z range of 200–2000.

X-ray Crystallography. Single-crystal X-ray data of both compounds, $[\text{CuL1}(\text{Cl})\cdot\text{H}_2\text{O}]$ ($\text{C}_{19}\text{H}_{15}\text{ClCuN}_6\text{O}_3$) and $[\text{Cu}(\text{NaL2})(\text{Cl})_2\cdot 2\text{H}_2\text{O}]$ ($\text{C}_{19}\text{H}_{17}\text{Cl}_2\text{Na}_{0.25}\text{CuN}_5\text{O}_5$) were collected on a Bruker AXS-KAPPA APEX II diffractometer, with graphite-monochromated Mo– $\text{K}\alpha$ radiation ($\lambda = 0.71073 \text{ \AA}$). The selected crystals of each compound were exposed for 10 s per frame, under cryo conditions (150 K) using an Oxford cryosystem, at 40 mm distance from the CCD. Each data set was integrated using the SAINT from Bruker AXS, with a multiscan absorption correction (SADABS). The structures were solved by direct methods with SHELXS⁷² and refined on F^2 using full-matrix least-squares with SHELXL,⁴⁸ through the WINGX-Version

1.70.01⁷³ package of programs. Data collection and refinement statistics are listed in Table 8. All non-hydrogen atoms were refined

Table 8. Crystal Data and Selected Refinement Details for Both Complexes

	[CuLi(Cl)]·H ₂ O	[Cu(NaL2)(Cl)]·2H ₂ O
empirical formula	C ₁₉ H ₁₃ ClCuN ₆ O ₂	C ₁₉ H ₁₈ ClCuN ₅ O ₆
FW	474.36	459.34
temperature (K)	150	150
crystal system	orthorhombic	orthorhombic
space group	P2 ₁ 2 ₁ 2 ₁	P2 ₁ 2 ₁ 2 ₁
cell dim (Å, deg)	<i>a</i> = 7.0381(5) <i>b</i> = 10.7231(8) <i>c</i> = 26.0409(16)	<i>a</i> = 7.5587(5) <i>b</i> = 10.9470(7) <i>c</i> = 23.1518(14)
<i>V</i> (Å ³)	1915.7(2)	1915.7
<i>Z</i>	4	4
ρ_{calc} (g cm ⁻³)	1.645	1.552
μ (mm ⁻¹)	0.834	1.278
<i>F</i> (000)	964	932
reflns collected	8840	10976
independent	4416	4747
reflns [<i>I</i> > 2 σ (<i>I</i>)]	3373	4049
no. of variables	287	263
<i>R</i> _{int}	0.0489	0.0475
final <i>R</i> indices [<i>F</i> ² > 2 σ (<i>F</i> ²)] ^a	<i>R</i> ₁ = 0.0475 <i>R</i> ₂ = 0.0933	<i>R</i> ₁ = 0.0546 <i>R</i> ₂ = 0.1566
<i>R</i> indices (all data) ^a	<i>R</i> ₁ = 0.0759 <i>R</i> ₂ = 0.1285	<i>R</i> ₁ = 0.0639 <i>R</i> ₂ = 0.1650

^a*R*₁ = $\sum ||F_o| - |F_c|| / \sum |F_o|$; *R*₂ = $\{\sum [w(F_o^2 - F_c^2)^2] / \sum [w(F_o^2)^2]\}^{1/2}$.

with anisotropic thermal displacement parameters except for the sodium ion modeled in the carboxylate ligand that is located in a special position. The majority of the hydrogen atoms were placed at calculated positions and refined using the riding model, except for those that could be positioned in agreement with the electron density peaks identified in the difference Fourier maps. These hydrogen atoms were then refined with individual isotropic temperature parameter. The analysis of the difference Fourier maps has also allowed the identification of solvent molecules in both ligands. In particular, in the [CuLi(Cl)]·H₂O complex, a water molecule could be modeled and its hydrogen atoms positioned in agreement to the difference Fourier maps. In the case of the [Cu(NaL2)(Cl)]·2H₂O complex, two water molecules and a sodium cation were modeled in agreement with the difference Fourier maps.

Cyclic Voltammetry. Cyclic voltammograms were taken on a BioLogic SP-150 potentiostat running with EC-Lab 5.40 software. The copper complexes and ligands were placed at 5.0×10^{-4} M in aqueous solution at pH 7.4 containing 0.1 M KNO₃ as supporting electrolyte. Before each measurement, solutions were saturated with Argon and afterward, a continuous Argon flow was kept on the top of the solution during all experiments. A three-electrode configuration cell was used, with a glassy carbon electrode as a working electrode, a platinum wire as auxiliary electrode, and as reference an Ag/AgCl electrode. Throughout the work all potentials will be referred to the Ag/AgCl electrode. The scan rate (*v*) varied between 50×10^{-3} and 0.5 V/s and the potential between 0.8 and -1.0 V. To ensure reproducible results before each set of experiments the glassy carbon electrode was carefully polished with alumina suspension (0.3 μ m) for 1 min and rinsed with Milli-Q water.

DFT Calculations. All theoretical calculations were performed with the ORCA program package.⁷⁴ Full geometry optimizations were carried out for all complexes using the GGA functional BP86^{75–77} in combination with the TZVP/P⁷⁸ basis set for all atoms and by taking advantage of the resolution of the identity (RI) approximation in the Split-RI-J variant⁷⁹ with the appropriate Coulomb fitting sets.⁸⁰ Increased integration grids (Grid4 in ORCA convention) and tight

SCF convergence criteria were used. Solvent effects were accounted for according to the experimental conditions. For that purpose, we used the water ($\epsilon = 80$) solvent within the framework of the conductor like screening (COSMO) dielectric continuum approach.⁸¹ Gibbs free energies were obtained from single-point calculations using the B3LYP^{82,83} functional together with the TZVP/P⁷⁸ basis set. They were computed from the gas-phase optimized structures as a sum of electronic energy, thermal corrections to free energy, and free energy of solvation. The thermodynamics of redox reactions is quantified by redox potentials, *E*, and are related to the Gibbs free energy change (ΔG^0) with $E = -\Delta G^0/nF$ where *n* is the number of electrons transferred in the cell and *F* is the Faraday constant. Theoretical predictions of redox potentials are based on the above equation and a common strategy for calculating the free energy change for redox reactions is based on a thermodynamic cycle linking the process in the gas phase with that in solvent as shown in Figure S11. The free energy change for the redox reaction, ΔG_{sol}^0 in solvent is computed from the free energy change of the gas-phase oxidation (or ionization) process (ΔG_{g}^0) and solvation free energies of the reduced/oxidized species ($\Delta G_{\text{s,rd}}^0$ and $\Delta G_{\text{s,ox}}^0$): $\Delta G_{\text{s}}^0 = \Delta G_{\text{g}}^0 + \Delta G_{\text{s,ox}}^0 - \Delta G_{\text{s,rd}}^0$. The Gibbs free energy change of the gas-phase ΔG_{g}^0 is computed from the gas-phase optimized structures as a sum of electronic energy, zero-point energy and thermal corrections. The connection between the gas and aqueous phases is made through the calculation of the solvation Gibbs free energy of the specific species. These terms were evaluated from the Gibbs free energy change of the system in vacuum and in solution using within the COSMO approach.^{79,40} All redox potentials are reported here as relative potentials referenced to a silver electrode (Ag/AgCl). The Ag/AgCl potential is 0.199 V more positive than that of the standard hydrogen electrode (SHE). Considering that the absolute potential of the SHE has been determined experimentally to be 4.43 eV, we have subtracted 4.23 V from the absolute potentials to make direct comparisons to experimental data referenced to the Ag/AgCl.^{84,85}

Cytotoxicity Assays. Cell Culture. The human ovarian cancer cell lines A2780 and A2870cisR (resistant to cisplatin) (ECACC, UK) were grown in RPMI 1640 culture medium (Invitrogen) supplemented with 10% FBS and 1% penicillin/streptomycin at 37 °C in a humidified atmosphere of 95% of air and 5% CO₂ (Heraeus, Germany). The human breast cancer cell line MCF7 were grown in DMEM culture medium (Invitrogen) supplemented with 10% FBS and 1% penicillin/streptomycin, in similar conditions as above.

Cytotoxicity Assay. The cytotoxicity of the complexes against the different cell lines was evaluated using a colorimetric method based on the tetrazolium salt MTT ([3-(4,5-dimethylthiazol-2-yl)-2,5-diphenyl-tetrazolium bromide], which is reduced by viable cells to yield purple formazan crystals. Cells were seeded in 96-well plates at a density of 1×10^4 to 1.5×10^4 cells per well in 200 μ L of culture medium and left to incubate overnight for optimal adherence. After careful removal of the medium, 200 μ L of a dilution series of 200 to 0.002 μ M of the compounds (stock solutions prepared fresh) in medium were added and incubation was performed at 37 °C/5% CO₂ for 72 h. The percentage of DMSO in cell culture medium did not exceed 1%. At the end of the incubation period, the compounds were removed and the cells were incubated with 200 μ L of MTT solution (500 μ g/mL). After 3–4 h at 37 °C/5% CO₂, the medium was removed and the purple formazan crystals were dissolved in 200 μ L of DMSO by shaking. The cell viability was evaluated by measurement of the absorbance at 570 nm using a plate spectrophotometer (Power Wave Xs, Bio-Tek). The cell viability was calculated dividing the absorbance of each well by that of the control wells. Each experiment was repeated at least two times and each point was determined in at least 4 replicates.

DNA Cleavage Activity. The plasmid DNA used for gel electrophoresis experiments was ϕ X174 (Promega). Linear DNA was obtained by digestion with the single-cutter restriction enzyme XhoI and used as a reference in agarose gel electrophoresis. DNA cleavage activity was evaluated by monitoring the conversion of supercoiled plasmid DNA (Sc, form I) to nicked circular DNA (Nck, form II) and linear DNA (Lin, form III).

Each reaction mixture was prepared by adding 6 μL of water, 2 μL (200 ng) of supercoiled DNA, 2 μL of 100 mM stock $\text{Na}_2\text{HPO}_4/\text{HCl}$ pH 7.2 buffer solution and 10 μL of the aqueous solution of the complex. The final reaction volume was 20 μL , the final buffer concentration was 10 mM and the final metal concentration varied from 10 to 250 μM . Samples were typically incubated for 18 h at 37 $^\circ\text{C}$, in the dark. When indicated, the reaction was carried out in the same buffer but in the presence of ascorbic acid (10 μM), H_2O_2 (50 μM), DMSO (5%) or in the dark.

After incubation, 6 μL of DNA loading buffer (0.05% bromophenol blue, 40% sucrose, 0.1 M H_4edta , pH 8.0, 0.5% sodium lauryl sulfate (SDS), Sigma) were added to each tube and the sample was loaded onto a 0.8% agarose gel in TBE buffer (89 mM Tris–borate, 1 mM H_4edta pH 8.3) containing ethidium bromide (0.5 $\mu\text{g}/\text{mL}$). Controls of nonincubated and of linearized plasmid were loaded on each gel electrophoresis. The electrophoresis was carried out for 2.5 h at 100 V. Bands were visualized under UV light and images captured using an AlphaImagerEP (Alpha Innotech). Peak areas were measured by densitometry using AlphaView Software (Alpha Innotech). Peak areas were used to calculate the percentage (%) of each form (Sc, Nck and Lin), with a correction factor of 1.47 for the Sc form to account for its lower staining capacity by ethidium bromide. The photos chosen were rearranged to show only the relevant samples. All samples in each figure were obtained from the same run.

■ ASSOCIATED CONTENT

■ Supporting Information

The Supporting Information is available free of charge on the ACS Publications website at DOI: 10.1021/acs.inorgchem.6b01884.

Crystallographic information file for CuL1 (CIF)

Crystallographic information file for CuL2 (CIF)

Experimental titration curves, species distribution diagrams for HL1, H_2L_2 , and their copper(II) complexes at different concentrations, EPR spectra at different pH values, ESI-MS spectra of copper(II) complexes, scheme of ligands and log K_{eff} graphics, cyclic voltammetry data at different scan rates, and Gibbs free energies for the gas-phase and solvated copper complexes (PDF)

■ AUTHOR INFORMATION

Corresponding Author

*E-mail: olga.iranzo@univ-amu.fr.

Present Addresses

[#]S.G.: Institut für Anorganische and Analytische Chemie, Friedrich-Schiller-Universität Jena, Humboldtstraße 8, 07743 Jena, Germany.

^{||}I.B.: European Molecular Biology Laboratory, Hamburg Outstation, Notkestrasse 85, 22607 Hamburg, Germany.

Notes

The authors declare no competing financial interest.

■ ACKNOWLEDGMENTS

O.I. acknowledge the financial support from the Fundação para a Ciência e a Tecnologia (FCT) (Pest-OE/EQB/LA0004/2011, the National Network of Mass Spectrometry REDE/1504/REM/2005, and the RECI/BBB-BQB/0230/2012 for the NMR spectrometers as part of the National NMR Facility) and from the European Commission (FP7-IRG-230896 Marie Curie grant). FCT is also acknowledged for grants SFRH/BPD/29564/2006 and SFRH/BPD/73361/2010 to S.G. and L.M.P.L., respectively, and FCT Investigator to F.M. S.G. also thanks the financial support from the Collaborative Research Centre ChemBioSys (CRC 1127) funded by the Deutsche

Forschungsgemeinschaft (DFG). M.C. Almeida from the Mass Spectrometry Service at the ITQB is acknowledged for providing ESI-MS data of the copper(II) complexes. Maria Teresa Duarte at Instituto Superior Técnico (IST) is sincerely acknowledged for support and for the provision of X-ray diffraction facilities.

■ REFERENCES

- (1) Pearson, R. G. *Hard and Soft Acids and Bases*. *J. Am. Chem. Soc.* **1963**, *85* (22), 3533–3539.
- (2) Frastão da Silva, J. J. R.; Williams, R. J. P. *The Biological Chemistry of the Elements: The Inorganic Chemistry of Life*; Oxford University Press: Oxford, NY, 2001.
- (3) Lippard, S. J.; Berg, J. M. *Principles of Bioinorganic Chemistry*; University Science Books: Mill Valley, CA, 1994.
- (4) Holm, R. H.; Kennepohl, P.; Solomon, E. I. Structural and Functional Aspects of Metal Sites in Biology. *Chem. Rev.* **1996**, *96* (7), 2239–2314.
- (5) Gaggelli, E.; Kozłowski, H.; Valensin, D.; Valensin, G. Copper Homeostasis and Neurodegenerative Disorders (Alzheimer's, Prion, and Parkinson's Diseases and Amyotrophic Lateral Sclerosis). *Chem. Rev.* **2006**, *106* (6), 1995–2044.
- (6) Kraatz, H.-B.; Metzler-Nolte, N. *Concepts and Models in Bioinorganic Chemistry*; Wiley-VCH: Weinheim, 2006.
- (7) Solomon, E. I.; Heppner, D. E.; Johnston, E. M.; Ginsbach, J. W.; Cirera, J.; Qayyum, M.; Kieber-Emmons, M. T.; Kjaergaard, C. H.; Hadt, R. G.; Tian, L. Copper Active Sites in Biology. *Chem. Rev.* **2014**, *114* (7), 3659–3853.
- (8) Halliwell, B.; Gutteridge, J. M. Role of free radicals and catalytic metal ions in human disease: An overview. *Methods in Enzymology: Oxygen Radicals in Biological Systems Part B: Oxygen Radicals and Antioxidants*; Academic Press, 1990; pp 1–85.
- (9) Peña, M. M. O.; Lee, J.; Thiele, D. J. A Delicate Balance: Homeostatic Control of Copper Uptake and Distribution. *J. Nutr.* **1999**, *129* (7), 1251–1260.
- (10) Wang, T.; Guo, Z. Copper in Medicine: Homeostasis, Chelation Therapy and Antitumor Drug Design. *Curr. Med. Chem.* **2006**, *13* (5), 525–537.
- (11) Wadas, T. J.; Wong, E. H.; Weisman, G. R.; Anderson, C. J. Coordinating Radiometals of Copper, Gallium, Indium, Yttrium, and Zirconium for PET and SPECT Imaging of Disease. *Chem. Rev.* **2010**, *110* (5), 2858–2902.
- (12) Tisato, F.; Marzano, C.; Porchia, M.; Pellei, M.; Santini, C. Copper in diseases and treatments, and copper-based anticancer strategies. *Med. Res. Rev.* **2010**, *30* (4), 708–749.
- (13) Duncan, C.; White, A. R. Copper complexes as therapeutic agents. *Metallomics* **2012**, *4* (2), 127–138.
- (14) Franz, K. J. Application of inorganic chemistry for non-cancer therapeutics. *Dalton Trans.* **2012**, *41* (21), 6333–6334.
- (15) Santini, C.; Pellei, M.; Gandin, V.; Porchia, M.; Tisato, F.; Marzano, C. Advances in Copper Complexes as Anticancer Agents. *Chem. Rev.* **2014**, *114* (1), 815–862.
- (16) Brissos, R. F.; Caubet, A.; Gamez, P. Possible DNA-Interacting Pathways for Metal-Based Compounds Exemplified with Copper Coordination Compounds. *Eur. J. Inorg. Chem.* **2015**, *2015* (16), 2633–2645.
- (17) Brandt, W. W.; Dwyer, F. P.; Gyarfas, E. D. Chelate Complexes of 1,10-Phenanthroline and Related Compounds. *Chem. Rev.* **1954**, *54* (6), 959–1017.
- (18) Sigel, H.; Martin, R. B. Coordinating properties of the amide bond. Stability and structure of metal ion complexes of peptides and related ligands. *Chem. Rev.* **1982**, *82* (4), 385–426.
- (19) Kozłowski, H.; Bal, W.; Dyba, M.; Kowalik-Jankowska, T. Specific structure–stability relations in metalloptides. *Coord. Chem. Rev.* **1999**, *184* (1), 319–346.
- (20) Kozłowski, H.; Kowalik-Jankowska, T.; Jeżowska-Bojczuk, M. Chemical and biological aspects of Cu²⁺ interactions with peptides

and aminoglycosides. *Coord. Chem. Rev.* **2005**, *249* (21–22), 2323–2334.

(21) Sigman, D. S.; Graham, D. R.; D'Aurora, V.; Stern, A. M. Oxygen-dependent cleavage of DNA by the 1,10-phenanthroline cuprous complex. Inhibition of *Escherichia coli* DNA polymerase I. *J. Biol. Chem.* **1979**, *254* (24), 12269–12272.

(22) Sigman, D. S.; Mazumder, A.; Perrin, D. M. Chemical nucleases. *Chem. Rev.* **1993**, *93* (6), 2295–2316.

(23) Ruiz-Ramírez, L.; de la Rosa, M. E.; Gracia-Mora, I.; Mendoza, A.; Pérez, G.; Ferrer-Sueta, G.; Tovar, A.; Breña, M.; Gutierrez, P.; Cruces Martínez, M. P.; Pimentel, E.; Natarajan, A. T. Casiopeínas, metal-based drugs a new class of antineoplastic and genotoxic compounds. *J. Inorg. Biochem.* **1995**, *59* (2–3), 207.

(24) Ruiz-Ramírez, L.; Gracia-Mora, I.; de la Rosa, M. E.; Sumano, H.; Gomez, C.; Arenas, F.; Gomez, E.; Pimentel, E.; Cruces, M. Cytostatic, mutagenic, antineoplastic activities and preliminary toxicity of copper (II) new drugs: Casiopeínas I, II, III. *J. Inorg. Biochem.* **1993**, *51* (1–2), 406.

(25) Alemón-Medina, R.; Breña-Valle, M.; Muñoz-Sánchez, J. L.; Gracia-Mora, M. I.; Ruiz-Azuara, L. Induction of oxidative damage by copper-based antineoplastic drugs (Casiopeínas®). *Cancer Chemother. Pharmacol.* **2007**, *60* (2), 219–228.

(26) Rivero-Müller, A.; de Vizcaya-Ruiz, A.; Plant, N.; Ruiz, L.; Dobrota, M. Mixed chelate copper complex, Casiopeína Igly®, binds and degrades nucleic acids: A mechanism of cytotoxicity. *Chem.-Biol. Interact.* **2007**, *165* (3), 189–199.

(27) Bravo-Gómez, M. E.; García-Ramos, J. C.; Gracia-Mora, I.; Ruiz-Azuara, L. Antiproliferative activity and QSAR study of copper(II) mixed chelate [Cu(N–N) (acetylacetonato)]NO₃ and [Cu(N–N) (glycinato)]NO₃ complexes, (Casiopeínas®). *J. Inorg. Biochem.* **2009**, *103* (2), 299–309.

(28) Ruiz-Azuara, L.; Bravo-Gomez, M. E. Copper Compounds in Cancer Chemotherapy. *Curr. Med. Chem.* **2010**, *17* (31), 3606–3615.

(29) Patra, A. K.; Nethaji, M.; Chakravarty, A. R. Red-light photosensitized cleavage of DNA by (L-lysine) (phenanthroline base)copper(II) complexes. *Dalton Trans.* **2005**, No. 16, 2798–2804.

(30) Patra, A. K.; Dhar, S.; Nethaji, M.; Chakravarty, A. R. Metal-assisted red light-induced DNA cleavage by ternary l-methionine copper(II) complexes of planar heterocyclic bases. *Dalton Trans.* **2005**, No. 5, 896–902.

(31) Patra, A. K.; Bhowmick, T.; Roy, S.; Ramakumar, S.; Chakravarty, A. R. Copper(II) Complexes of l-Arginine as Netropsin Mimics Showing DNA Cleavage Activity in Red Light. *Inorg. Chem.* **2009**, *48* (7), 2932–2943.

(32) Patra, A. K.; Bhowmick, T.; Ramakumar, S.; Nethaji, M.; Chakravarty, A. R. DNA cleavage in red light promoted by copper(ii) complexes of [small alpha]-amino acids and photoactive phenanthroline bases. *Dalton Trans.* **2008**, No. 48, 6966–6976.

(33) Goswami, T. K.; Chakravarthi, B. V. S. K.; Roy, M.; Karande, A. A.; Chakravarty, A. R. Ferrocene-Conjugated l-Tryptophan Copper(II) Complexes of Phenanthroline Bases Showing DNA Photocleavage Activity and Cytotoxicity. *Inorg. Chem.* **2011**, *50* (17), 8452–8464.

(34) Rao, R.; Patra, A. K.; Chetana, P. R. DNA binding and oxidative cleavage activity of ternary (L-proline)copper(II) complexes of heterocyclic bases. *Polyhedron* **2007**, *26* (18), 5331–5338.

(35) Rao, R.; Patra, A. K.; Chetana, P. R. Synthesis, structure, DNA binding and oxidative cleavage activity of ternary (L-leucine/isoleucine) copper(II) complexes of heterocyclic bases. *Polyhedron* **2008**, *27* (5), 1343–1352.

(36) Chetana, P. R.; Rao, R.; Roy, M.; Patra, A. K. New ternary copper(II) complexes of l-alanine and heterocyclic bases: DNA binding and oxidative DNA cleavage activity. *Inorg. Chim. Acta* **2009**, *362* (13), 4692–4698.

(37) Chetana, P. R.; Rao, R.; Saha, S.; Policegoudra, R. S.; Vijayan, P.; Aradhya, M. S. Oxidative DNA cleavage, cytotoxicity and antimicrobial studies of l-ornithine copper (II) complexes. *Polyhedron* **2012**, *48* (1), 43–50.

(38) LakshmiPraba, J.; Arunachalam, S.; Gandhi, D. A.; Thirunalasundari, T. Synthesis, nucleic acid binding and cytotoxicity

of polyethyleneimine-copper(II) complexes containing 1,10-phenanthroline and L-valine. *Eur. J. Med. Chem.* **2011**, *46* (7), 3013–3021.

(39) Jia, L.; Jiang, P.; Xu, J.; Hao, Z.-y.; Xu, X.-m.; Chen, L.-h.; Wu, J.-c.; Tang, N.; Wang, Q.; Vittal, J. J. Synthesis, crystal structures, DNA-binding properties, cytotoxic and antioxidation activities of several new ternary copper(II) complexes of N,N'-(p-xylylene)di-alanine acid and 1,10-phenanthroline. *Inorg. Chim. Acta* **2010**, *363* (5), 855–865.

(40) Kumar, R. S.; Arunachalam, S. DNA binding and antimicrobial studies of polymer-copper(II) complexes containing 1,10-phenanthroline and L-phenylalanine ligands. *Eur. J. Med. Chem.* **2009**, *44* (5), 1878–1883.

(41) Zhang, S.; Zhu, Y.; Tu, C.; Wei, H.; Yang, Z.; Lin, L.; Ding, J.; Zhang, J.; Guo, Z. A novel cytotoxic ternary copper(II) complex of 1,10-phenanthroline and L-threonine with DNA nuclease activity. *J. Inorg. Biochem.* **2004**, *98* (12), 2099–2106.

(42) Ramakrishnan, S.; Rajendiran, V.; Palaniandavar, M.; Periasamy, V. S.; Srinag, B. S.; Krishnamurthy, H.; Akbarsha, M. A. Induction of Cell Death by Ternary Copper(II) Complexes of l-Tyrosine and Diimines: Role of Coligands on DNA Binding and Cleavage and Anticancer Activity. *Inorg. Chem.* **2009**, *48* (4), 1309–1322.

(43) Chan, W. C.; White, P. D. *Fmoc Solid Phase Peptide Synthesis: A Practical Approach*; Oxford University Press: New York, 2000.

(44) Sun, W.-H.; Jie, S.; Zhang, S.; Zhang, W.; Song, Y.; Ma, H.; Chen, J.; Wedeking, K.; Fröhlich, R. Iron Complexes Bearing 2-Imino-1,10-phenanthroline Ligands as Highly Active Catalysts for Ethylene Oligomerization. *Organometallics* **2006**, *25* (3), 666–677.

(45) Pettit, L. D.; Powell, H. K. J. *IUPAC Stability Constants Database*; Academic Software: Timble, U.K., 2003.

(46) Anderegg, G.; Wanner, H. Pyridine derivatives as complexing agents. XIII. The stability of the palladium(II) complexes with pyridine, 2,2'-bipyridyl, and 1,10-phenanthroline. *Inorg. Chim. Acta* **1986**, *113* (2), 101–108.

(47) Lima, L. M. P.; Halime, Z.; Marion, R.; Camus, N.; Delgado, R.; Platas-Iglesias, C.; Tripier, R. Monopicolinate Cross-Bridged Cyclam Combining Very Fast Complexation with Very High Stability and Inertness of Its Copper(II) Complex. *Inorg. Chem.* **2014**, *53* (10), 5269–5279.

(48) Alderighi, L.; Gans, P.; Ienco, A.; Peters, D.; Sabatini, A.; Vacca, A. Hyperquad simulation and speciation (HySS): a utility program for the investigation of equilibria involving soluble and partially soluble species. *Coord. Chem. Rev.* **1999**, *184* (1), 311–318.

(49) Formicka-Kozłowska, G.; Bezer, M.; Pettit, L. D. Coordination ability of the thyrotropin releasing factor, L-pyroglutamyl-L-histidyl-L-prolinamide(TRF).III. Cu(II) and Ni(II) complexes with TRF and its di- and tripeptide analogues. *J. Inorg. Biochem.* **1983**, *18* (4), 335–347.

(50) Gasque, L.; Moreno-Esparza, R.; Ruiz-Ramírez, L. Stability of ternary copper and nickel complexes with 1,10-phenanthroline. *J. Inorg. Biochem.* **1992**, *48* (2), 121–127.

(51) Hendrich, M. P. *SpinCount Software*; Carnegie Mellon University: Pittsburgh, PA.

(52) Peisach, J.; Blumberg, W. E. Structural implications derived from the analysis of electron paramagnetic resonance spectra of natural and artificial copper proteins. *Arch. Biochem. Biophys.* **1974**, *165* (2), 691–708.

(53) García-Ramos, J. C.; Galindo-Murillo, R.; Tovar-Tovar, A.; Alonso-Saenz, A. L.; Gómez-Vidales, V.; Flores-Álamo, M.; Ortiz-Frade, L.; Cortes-Guzmán, F.; Moreno-Esparza, R.; Campero, A.; Ruiz-Azuara, L. The π -Back-Bonding Modulation and Its Impact in the Electronic Properties of CuII Antineoplastic Compounds: An Experimental and Theoretical Study. *Chem. - Eur. J.* **2014**, *20* (42), 13730–13741.

(54) Sakaguchi, U.; Addison, A. W. Spectroscopic and redox studies of some copper(II) complexes with biomimetic donor atoms: implications for protein copper centres. *J. Chem. Soc., Dalton Trans.* **1979**, No. 4, 600–608.

(55) Burnett, M. N.; Johnson, C. K. *ORTEP-III Oak Ridge Thermal Ellipsoid Plot Program for Crystal Structure Illustrations*; Oak Ridge National Laboratory Report ORNL-6895, 1996.

- (56) Solans, X.; Ruiz-Ramirez, L.; Martinez, A.; Gasque, L.; Moreno-Esparza, R. Mixed chelate complexes. II. Structures of L-alaninato-(aqua)(4,7-diphenyl-1,10-phenanthroline)copper(II) nitrite monohydrate and aqua(4,7-dimethyl-1,10-phenanthroline) (glycinato) (nitrate)copper(II) monohydrate. *Acta Crystallogr., Sect. C: Cryst. Struct. Commun.* **1993**, *49* (5), 890–893.
- (57) Alvarez-Larena, A.; Brioso-Penalva, J. L.; Piniella, J. F.; Moreno-Esparza, R.; Ruiz-Ramirez, L.; Ferrer-Sueta, G. Aqua(glycinato)(3,4,7,8-tetramethyl-1,10-phenanthroline)copper(II) Nitrate. *Acta Crystallogr., Sect. C: Cryst. Struct. Commun.* **1995**, *51* (5), 852–854.
- (58) Moreno-Esparza, R.; Molins, E.; Brioso-Penalva, J. L.; Ruiz-Ramirez, L.; Redon, R. Aqua(1,10-phenanthroline)(L-serinato)copper(II) Nitrate. *Acta Crystallogr., Sect. C: Cryst. Struct. Commun.* **1995**, *51* (8), 1505–1508.
- (59) Gasque, L.; Moreno-Esparza, R.; Ruiz-Ramirez, L.; Medina-Dickinson, G. (5,6-Dimethyl-1,10-phenanthroline) (nitrate) (salicylaldehydato)copper(II). *Acta Crystallogr., Sect. C: Cryst. Struct. Commun.* **1999**, *55* (7), 1063–1065.
- (60) Gasque, L.; Moreno-Esparza, R.; Ruiz-Ramirez, L.; Medina-Dickinson, G. Aqua(4,7-diphenyl-1,10-phenanthroline) (salicylaldehydato)copper(II) nitrate monohydrate. *Acta Crystallogr., Sect. C: Cryst. Struct. Commun.* **1999**, *55* (7), 1065–1067.
- (61) Bard, A. J.; Faulkner, L. R. *Electrochemical Methods: Fundamentals and Applications*; Wiley: New York, 1980.
- (62) Rorabacher, D. B. Electron Transfer by Copper Centers. *Chem. Rev.* **2004**, *104* (2), 651–698.
- (63) Miyake, N.; Otsuka, Y.; Kurata, T. Autoxidation Reaction Mechanism for L-Ascorbic Acid in Methanol without Metal Ion Catalysis. *Biosci., Biotechnol., Biochem.* **1997**, *61* (12), 2069–2075.
- (64) Barycki, J. J.; Asard, H.; Stone, J. M.; Wilson, M. A.; Banerjee, R.; Becker, D. F. Antioxidant Molecules and Redox Cofactors. *Redox Biochemistry*; John Wiley & Sons, Inc, 2007; pp 11–47.
- (65) Lee, W. Y.; Yan, Y. K.; Lee, P. P. F.; Tan, S. J.; Lim, K. H. DNA binding and nucleolytic properties of Cu(II) complexes of salicylaldehyde semicarbazones. *Metallomics* **2012**, *4* (2), 188–196.
- (66) Gama, S.; Mendes, F.; Marques, F.; Santos, I. C.; Carvalho, M. F.; Correia, I.; Pessoa, J. C.; Santos, I.; Paulo, A. Copper(II) complexes with tridentate pyrazole-based ligands: synthesis, characterization, DNA cleavage activity and cytotoxicity. *J. Inorg. Biochem.* **2011**, *105* (5), 637–644.
- (67) Kaiser, E.; Colescott, R. L.; Bossinger, C. D.; Cook, P. I. Color test for detection of free terminal amino groups in the solid-phase synthesis of peptides. *Anal. Biochem.* **1970**, *34* (2), 595–598.
- (68) Schwarzenbach, G.; Flaschka, H. A. *Complexometric Titrations*; Methuen: London, 1969.
- (69) Rossotti, F. J. C.; Rossotti, H. Potentiometric titrations using Gran plots: A textbook omission. *J. Chem. Educ.* **1965**, *42* (7), 375.
- (70) Fragoso, A.; Lamosa, P.; Delgado, R.; Iranzo, O. Harnessing the Flexibility of Peptidic Scaffolds to Control their Copper(II)-Coordination Properties: A Potentiometric and Spectroscopic Study. *Chem. - Eur. J.* **2013**, *19* (6), 2076–2088.
- (71) Gans, P.; Sabatini, A.; Vacca, A. Investigation of equilibria in solution. Determination of equilibrium constants with the HYPERQUAD suite of programs. *Talanta* **1996**, *43* (10), 1739–1753.
- (72) Sheldrick, G. A short history of SHELX. *Acta Crystallogr., Sect. A: Found. Crystallogr.* **2008**, *64* (1), 112–122.
- (73) Farrugia, L. WinGX suite for small-molecule single-crystal crystallography. *J. Appl. Crystallogr.* **1999**, *32* (4), 837–838.
- (74) Neese, F. The ORCA program system. *WIREs Comput. Mol. Sci.* **2012**, *2* (1), 73–78.
- (75) Perdew, J. P. Density-functional approximation for the correlation energy of the inhomogeneous electron gas. *Phys. Rev. B: Condens. Matter Mater. Phys.* **1986**, *33* (12), 8822–8824.
- (76) Perdew, J. P. Erratum: Density-functional approximation for the correlation energy of the inhomogeneous electron gas. *Phys. Rev. B: Condens. Matter Mater. Phys.* **1986**, *34* (10), 7406.
- (77) Becke, A. D. Density-functional exchange-energy approximation with correct asymptotic behavior. *Phys. Rev. A: At., Mol., Opt. Phys.* **1988**, *38* (6), 3098–3100.
- (78) Schäfer, A.; Huber, C.; Ahlrichs, R. Fully optimized contracted Gaussian basis sets of triple zeta valence quality for atoms Li to Kr. *J. Chem. Phys.* **1994**, *100* (8), 5829–5835.
- (79) Neese, F. An improvement of the resolution of the identity approximation for the formation of the Coulomb matrix. *J. Comput. Chem.* **2003**, *24* (14), 1740–1747.
- (80) Weigend, F. Accurate Coulomb-fitting basis sets for H to Rn. *Phys. Chem. Chem. Phys.* **2006**, *8* (9), 1057–1065.
- (81) Klamt, A.; Schuurmann, G. COSMO: a new approach to dielectric screening in solvents with explicit expressions for the screening energy and its gradient. *J. Chem. Soc., Perkin Trans. 2* **1993**, No. 5, 799–805.
- (82) Becke, A. D. A new mixing of Hartree–Fock and local density-functional theories. *J. Chem. Phys.* **1993**, *98* (2), 1372–1377.
- (83) Lee, C.; Yang, W.; Parr, R. G. Development of the Colle-Salvetti correlation-energy formula into a functional of the electron density. *Phys. Rev. B: Condens. Matter Mater. Phys.* **1988**, *37* (2), 785–789.
- (84) Wang, T.; Brudvig, G.; Batista, V. S. Characterization of Proton Coupled Electron Transfer in a Biomimetic Oxomanganese Complex: Evaluation of the DFT B3LYP Level of Theory. *J. Chem. Theory Comput.* **2010**, *6* (3), 755–760.
- (85) Reiss, H.; Heller, A. The absolute potential of the standard hydrogen electrode: a new estimate. *J. Phys. Chem.* **1985**, *89* (20), 4207–4213.